Nationaal Lucht- en Ruimtevaartlaboratorium
National Aerospace Laboratory NLR

NLR-TP-99353

Unsolved aerospace heat and mass transfer research issues for the development of two-phase thermal control systems for space

A.A.M. Delil

Nationaal Lucht- en Ruimtevaartlaboratorium
National Aerospace Laboratory NLR

NLR-TP-99353

Unsolved aerospace heat and mass transfer research issues for the development of two-phase thermal control systems for space

A.A.M. Delil

Updated version of NLR TP 98170, presented as Invited Lecture at the Workshop on Non-Compression Refrigeration & Cooling, Odessa, Ukraine, 7-11 June 1999.

Division:	Space
Issued:	May 1999
Classification of title:	Unclassified

Contents

1 Table
21 Figures

(26 pages in total)

This page is intentionally left blank.

UNSOLVED AEROSPACE HEAT AND MASS TRANSFER RESEARCH ISSUES FOR THE DEVELOPMENT OF TWO-PHASE THERMAL CONTROL SYSTEMS FOR SPACE

A.A.M. DELIL
National Aerospace Laboratory NLR, Space Division
P.O. Box 153, 8300 AD Emmeloord, The Netherlands

ABSTRACT

This review concerns heat and mass transfer research issues pertaining to the current development of active thermal control systems for spacecraft, i.e. the development of two-phase heat transport system technology. Various topics are discussed to show that many investigations are being done to solve the different problems. The progress is discussed, including current activities and work to be done. The discussions focus on the development and in-orbit technology demonstration of Capillary Pumped Loops and Loop Heat Pipes and on thermal/gravitational scaling of two-phase heat transport systems. They include also the prediction of gravity level dependent adiabatic and condensing flow behaviour, creation of gravity level dependent two-phase flow regime (pattern) maps, and development of two-phase thermal management systems components, like vapour quality sensors, high efficiency low pressure drop condensers and rotatable thermal joints.

1. INTRODUCTION

Space-related heat and mass transfer problems originate from:

- Absence of gravity induced behaviour differing from the normal behaviour on earth, e.g. boiling, condensation, two-phase flow and heat transport, flow pattern maps, capillary electrophoresis, melting, solidification, crystal growth, critical point phenomena.
- Passive or active thermal control of a variety of spacecraft: earth orbiting satellites, solar and deep space probes, satellites to and possibly landing on moon, planets or comets.
- Hostile environments, being vibrations during the launch, aerodynamic heating during ascent and descent, meteoroids impingement, vacuum, atomic oxygen, and incident radiation (UV, X-ray, particles).

To solve these problems research has been, is and will be carried out concerning:

- Passive thermal control, including the thermophysical properties of new thermal or structural materials or components: anisotropic (sheet) materials, metal and carbon fibre honeycomb sandwich panels, multilayer insulation blankets, thermal joints and interface fillers, phase change materials for thermal storage systems, heat pipes and thermo-optical coatings for radiators.
- Active thermal control, using Variable Conductance Heat Pipes (VCHP), novel heat pipes (e.g. the Electro Hydro Heat Dynamic Pipe, EHDHP), Loop Heat Pipes (LHP), Mechanically Pumped and Capillary Pumped two-phase Loops (MPL & CPL) and their components (Vapour Quality Sensors, evaporators, condensers, valves, control reservoirs, control algorithms), electrochromic radiator coatings, louvres, flexible thermal links and rotatable thermal joints for deployable and steerable radiators.
- Thermal/gravitational modelling and scaling of two-phase heat transport systems to be used to design spacecraft systems, using terrestrial test data.
- Experiments in low-gravity environments (in drop towers, during low-g aircraft flights, in sounding rockets, or in orbit). Experiments, dealing with pool boiling and Marangoni convection, were done during International Micro-gravity Laboratory, US Micro-gravity Payload and EUropean REtrievable CArrier flights.
- Other experiments were done to demonstrate two-phase technology in orbit: ESA's two-phase experiments TPX I&II, NASA's capillary pumped loop experiments CAPL 1&2&3 and the Two-Phase Flow Thermal Control Experiment TPF, the all-American loop heat pipe experiment ALPHA, the loop heat pipe flight experiment LHPFX, the Cryogenic Capillary Pumped Loop Flight Experiment CCPL and the Russian experiments Mars 94 & 96, Valentina and Tatyana.

The different topics described on the next pages will concentrate on the development and in-orbit demonstration of two-phase heat transport systems and their components, including design supporting theoretical activities, like thermal gravitational modelling and scaling of such systems and the assessment of gravity level dependent two-phase adiabatic flow, condensation behaviour and flow pattern mapping.

2. TWO-PHASE HEAT TRANSPORT SYSTEM TECHNOLOGY

Thermal management systems for future large spacecraft must be able to transport large amounts of dissipated power (up to say 200 kW), over large distances (up to say 100 metres). Conventional single-phase systems (based on the heat capacity of the working fluid) are simple, well understood, easy to test, relatively inexpensive and low risk. But in order to realise a proper thermal control task with small temperature drops from equipment to radiator (to limit radiator size and mass), they require noisy, heavy, high power pumps and consequently large solar arrays.

2.1 Mechanically Pumped Systems

As an alternative for these single-phase systems one currently considers mechanically pumped two-phase systems, accepting heat by evaporation of the working fluid at heat dissipating stations (cold plates, heat exchangers), releasing heat by condensation at heat demanding stations (hot plates, heat exchangers) and at radiators, for rejection into space. Such systems, relying on the heat of vaporisation, operate nearly isothermally. Pumping power is reduced by orders of magnitude, thus minimising radiator and solar array sizes.

The stations can be arranged in a pure series, pure parallel or hybrid configuration. The series configuration is the simplest, it offers the possibility of heat load sharing between the different stations, with some restrictions with respect to their sequence in the loop. However, the series configuration has very limited growth potential and the higher flow resistance.

In the low resistance, modular, parallel concept, the stations operate relatively independently, thus offering full growth capability. However, the parallel configuration is more complicated, especially when redundancy and heat load sharing (some cold plates operating in reverse mode) is foreseen. In addition, a parallel configuration requires a control system consisting of various sensors, monitoring the loop performance at different locations, control logic and actuators to adjust e.g. pump speed, fluid reservoir content and throughputs of valves. Sensors for control are pressure gauges, flow meters, temperature gauges and vapour quality sensors, measuring the relative vapour mass content of the flowing mixture. An important application for vapour quality sensors (VQS) is at the cold plate exits, as a part of a control (sub-)system, adjusting the liquid fed into the cold plate to prevent the dry-out of the evaporator, or maintaining a prescribed quality value at evaporator exits, independent from transient heat sources and heat sink conditions (Delil, 1988).

ESA´s mechanically pumped two-phase loop activities have led to the definition of a Two-Phase Heat Transport System, TPHTS (Siepmann et al., 1992) and to the identification and development of various components considered to be critical for two-phase applications. These critical components were extensively and successfully tested in a R114 technology development two-phase test bed (Dunbar et al., 1990). Examples of these components are: A newly developed multi-channel condenser and a VQS, designed as an axial field capacitance meter, measuring the differences in dielectric permittivity of vapour and liquid (Siepmann et al., 1992; Delil, 1998).

2.2 Capillary Pumped Systems

An alternative for the mechanically pumped system is the capillary pumped system, using surface tension induced pumping action of capillary-type evaporators. Such capillary two-phase systems can be applied for instance in spacecraft not allowing vibrations (induced by mechanical pumping). Ammonia is the most promising candidate working fluid for capillary two-phase thermal control loops.

Two different systems can be distinguished (Cullimore & Nikitkin, 1998) : the western - heritage Capillary Pumped Loop (Stenger, 1966; Cullimore, 1993) and the Russian-heritage Loop Heat Pipe (Bienert & Wolf, 1995; Maidanik et al., 1991&1995). Although initially perceived by many as alternatives to heat pipes at high transport powers (>500W, up to 24kW), in recent years the intrinsic advantages of a small-diameter piping system without distributed wick structures have been exploited at low powers (20 to 100W). Many CPL and LHP advantages are only truly exploited when these devices are considered early in the design, rather than treated as replacement for existing heat pipe based design.

Advantages of a CPL and a LHP are:

- The tolerance of large adverse tilts (meaning a heat source up to 4 m above a heat sink, facilitating ground testing and even enabling many terrestrial applications).
- Tolerance of complicated layouts/tortuous transport paths.
- Easy accommodation of flexible sections, make/break joints, and vibration isolation.
- Fast and strong diode action.
- Straightforward application in either fixed conductance or variable conductance modes.
- Separation of heat acquisition and rejection components for independent optimisation of heat transfer footprints and even integral independent bonding of such components in larger structures.
- Accommodation of mechanical pumps.
- An apparent tolerance of large amounts of non-condensible gases which means extended lifetime.

Because of their performance advantages, unique operational characteristics, and recent successful flight experiments, CPL and LHP technologies are currently gaining acceptance in the aerospace community. They are baselined for several missions including NASA's EOS-AM, JPL's MSP ("Mars '98"), ESA's ATLID, CNES's STENTOR, RKA's OBZOR and MARS 96 mission, a retrofit mission for the Hubble space telescope, COMET, the Hughes 702 satellites, and various other commercial geo-synchronous communication satellites.

3. IN-ORBIT TECHNOLOGY DEMONSTRATION

As two-phase flow characteristics and heat transfer differ when subjected to a 1-g or a low-gravity environment, the technology of two-phase heat transport systems including their components was to be demonstrated in orbit. Therefore several in-orbit experiments were recently carried out: ESA's Two-Phase eXperiment TPX I, NASA's CApillary Pumped Loop experiments CAPL 1&2 (Butler et al., 1996; Ku et al., 1995), the Loop Heat Pipe Flight eXperiment LHPFX, the ALPHA experiment (Haught & Cullimore, 1998) and the Two-Phase Flow experiment TPF (Ottenstein & Nienberg, 1998; Antoniuk & Nienberg, 1998). Others are planned for near-term space flights: TPX II, CAPL 3 (Ku et al., 1998; Kim et al, 1997), STENTOR (Amadieu et al., 1997), the Cryogenic CCPL (Hagood, 1998), the Two-phase Extended Evaluation in Micro-gravity experiment TEEM (Miller-Hurlbert, 1997), and Granat (Orlov et al., 1997). Detailed discussions are given next on experiments with NLR involvement, TPX I&II and LHPFX.

3.1 TPX I

TPX I development (Delil et al., 1995) started in 1990, by NLR (prime contractor), SABCA, Fokker Space, Bradford and Stork Products Engineering. This flight experiment was a scaled-down capillary pumped two-phase ammonia system, containing some scaled-down components of a mechanically pumped loop: multichannel condensers, vapour quality sensors and a controllable three-way valve. TPX has run autonomously in Get Away Special G557 on Space Shuttle STS-60 (Feb. 1994), using own power supply, data handling and experiment control.

The experiment schematic (Delil et al., 1995) is shown in figure 1a. Heat, supplied to two parallel capillary pumped evaporators (a flat and a cylindrical one), causes evaporation of the working fluid, sets the mass flow rate and generates the pumping pressure to maintain the working fluid circulation in the system. The heat, extracted from the fluid in the condenser sections and sub-cooler, is dumped to space via the GAS canister lid. The control of the loop temperature set-point is by a Peltier element controlling an accumulator (reservoir), which contains liquid and vapour in equilibrium. In addition, the loop contains two vapour quality sensors, a controllable three-way valve with a vapour bypass line, and de-priming heaters for the two evaporators. The complete experiment had to fulfil the GAS requirements and restrictions: allowable volume (135 litres) and mass (90 kg maximum), no power and data communication connections to STS (hence limited battery energy and internal data storage), Shuttle attitude dependent thermal sink conditions and limited crew action (only on/off).

The TPX I baseline had to meet the many objectives for the different experiment constituents: capillary pumped loop (CPL), vapour quality sensors (VQS) and multichannel condensers, each of them being a scaled-down version of the concept developed for power systems up to 10 kW. The downscaling was intended not to affect the goals of the in-orbit demonstration of these concepts.

CPL objectives were to demonstrate in low-gravity:
- The capability to smoothly/continuously transport heat.
- Proper operation for different heat loads applied to two evaporators in parallel.
- The capability to share heat load between the evaporators, to maintain a constant and homogeneous temperature.
- The capability to prime an evaporator by a controlled management of the reservoir fluid content.
- The capability to start-up from low temperatures.
- The capability to control a set-point temperature (while operating under different, varying heat load and sink conditions) by proper reservoir fluid content control.

Within the CPL two evaporators, a cylindrical and a flat one, were present to determine in low-g:
- Transport capabilities and maximum pumping pressures.
- De-priming/re-priming by controlled reservoir actions.
- Evaporator heat transfer coefficients.
- The interaction of evaporators in parallel, also with respect to heat load sharing.

An additional, for future CPL design very important, objective was to assess and compare the (limits of the) CPL heat transport capability under low gravity and terrestrial conditions and to compare these with predictions resulting from modelling with thermal analyzer program ESATAN.

Incorporation of two VQS had several objectives:
- To prove the feasibility of the concept in space.
- To demonstrate proper VQS performance for ammonia, the most promising working fluid for space systems.
- To compare the performance of the two sensors in order to assess the influence of the location within the loop and of small construction differences.
- To perform calibrations and to assess differences in low-g and terrestrial sensor performances (important for design of future space-oriented vapour quality sensors).
- To carry out vapour quality control exercises to prove the usefulness of VQS for system control and to demonstrate the proper performance of the controllable three-way valve.

The multichannel condenser design objectives can be summarised by: demonstration/verification of the working principle and determination of the performance limits in a low-gravity environment (aspects of power transported, pressure drop, distribution of the fluid over the different channels and prevention of channel blockage included).

An extra objective was the use of low-g and one-g TPX I test data and outcomes of testing in two-phase test loops, to verify the NLR approach for thermal-gravitational scaling of two-phase flow and heat transfer (Delil, 1991, 1992, 1998), discussed later in this paper.

To fulfil the objectives an extended experimental programme was carried out, until battery exhaust. This in-flight testing included the following experiments:
- Balanced power: same power fed to both evaporators.
- Unbalanced power profile: different power levels fed to the two evaporators, to study mutual interaction.
- Heat load sharing: heat load applied only to one evaporator, the second acting as condenser.
- De-priming/re-priming by a special heater, shortly powered to induce an evaporator dry-out, followed by a re-priming action using the reservoir.
- Transient behaviour: a step change in the applied power to one evaporator in a steady-state system situation.
- Start-up behaviour.
- Loop temperature control: maintenance of the loop set-point and a controlled change of set-point levels.
- Vapour quality set-point control: control of bypass valve setting to maintain set vapour qualities in the VQS.
- System control: maintain (by accumulator and bypass valve control) the set-point values of the loop saturation temperature and vapour quality at the mixing point, under changing heat loads or sink temperatures.
- Extreme conditions: to assess limits of performance.

The best test sequence for above experiments had been predefined, based on extensive ground testing and modelling. In general: low power tests, to be done when the battery temperature is too low for high power supply, could be used to increase the battery temperature to a level that allows the battery to supply more power to the experiment. High power tests were preferably to be done in the first part of the experiment duration, as this allows the addition of some extra low power experimental cycles.

The configuration is shown in figure 2. It consists of a structure of four columns and three parallel plates:
- One, at one end of the columns, accommodating the

battery and the electronics hardware at either side.
- One, the loop plate, at the other end of the columns, attached in a well conductive manner to the canister lid and accommodating most CPL components.
- One, accommodating the evaporators, thermally de-coupled between the others, 40 mm from the base plate.

Materials used: Al 7075 for structure components (except evaporator plate: polycarbonate). Al 6061 for tubing and components, except the flow meters being stainless steel.

The flat evaporator consists of a (heated) base plate with microchannels for vapour flow, a 30 μm porous polyethylene wick with an inlet hole for the liquid, and a box shell which has been electron beam welded to the base plate, having an inlet liquid tube, teflon insulator and outlet vapour tube. Measured performances/characteristics are: Heat load: 155 W maximum, minimum: 8.8 W, Capillary pressure (ammonia): 2933 Pa, Pumping pressure at 155 W: 2200 Pa, Burst pressure: 260 Bar, Mass: 0.6 kg.

The cylindrical evaporator consists of a cylindrical (heated) shell with inner circular grooves for the vapour flow, a liquid inlet tube with teflon insulation, an outlet vapour tube and a 30 μm porous polyethylene rod with vapour collecting grooves and an inlet hole for the liquid. Measured performances and characteristics: Maximum heat load: 400 W, Minimum heat load: 7.7 W, Capillary static pressure (ammonia): 2707 Pa, Pumping pressure at 150 W: 1800 Pa, Burst pressure: >200 Bar, Mass 0.28 kg.

The control reservoir is a cylindrical vessel with an inlet/outlet (liquid) tube, a liquid/vapour separating 30 μm polyethylene wick, an acquisition (flower shape) wick and a cover welded on the vessel, equipped with two Peltier elements and a copper braid connected to the condenser inlet. Measured performances and characteristics: Liquid content 0.17 litre, Peltier control power 4.7 W maximum, Mass: 0.92 kg, Burst pressure: 275 Bar, Temperature control accuracy: 0.1 K in the range 263 to 323 K.

Two Liquid Flow Meters (LFM) were in the loop:
- To measure the total mass flow rate (redundant) during experiments with closed condenser bypass.
- To assess the bypass line flow rate (by subtracting the two LFM rates), to obtain the vapour quality at the mixture point for VQS calibration and control exercises.

Two VQS were in the loop. A VQS consists of a glass tube, with the glass covered capacitor electrodes on the internal wall, surrounded by a stainless steel envelope for strength reasons, the sensor electronics on top of it.

The Data Acquisition and Control (DAC) system included all electric/electronic hardware and the software for testing and operating the TPX I, for storing measured data, and for retrieval of the experimental data. The DAC flight-hardware included a Battery Pack, Cable Harness, and Payload Measurements and Control Unit (PMCU). The battery, selected to provide the power for the experiment during the flight, was a modified MAUS battery pack specified to offer at least 1800 Whrs @ 28.5 V DC. The PMCU was the on-board control box for experiment execution and safe-guarding, sensor measurements, actuator control, data storage and communication with Electrical Ground Support Equipment. To receive all information about the performance of the loop and components (location of condensation front, degree of sub-cooling, loop set point, evaporator temperature distribution and pressure drop, reservoir temperature and sink temperature distribution), the following parameters were measured: temperatures (38), flow rates (2), vapour qualities (2), the absolute vapour pressure, the pressure drop across the evaporators, the valve position, evaporator heater currents (2), de-priming heater currents (2) and the Peltier current.

The DAC software consisted of on-board (embedded) software and EGSE software. As operational behaviour and details about parameters of the experiment were test sequence (resulting from actual in-orbit conditions) dependent, the embedded software has been split into a fixed program and a set of experimenter defined tables, without compromising the reliability of the software. Major functions of the embedded software pertained to experiment planning, data acquisition from all sensors, execution of specified control algorithms, actuator control, data recording & safeguarding.

1.9 Mb data was stored before battery exhaust. The total experiment time was more than 40 hours. The general conclusion was that TPX I (the loop and all components, except the differential pressure sensor) functioned properly, without ammonia leakage or failures.

The flight data proved that the CPL showed:
- Proper start-up at various power levels.
- The capability to transport heat smoothly/continuously.
- Proper operation of two evaporators in parallel.
- Proper heat load sharing between the evaporators, with the ability of the loop to maintain a smooth operation.
- The ability to adjust/maintain a set point temperature with an accuracy of better than say 0.3 K, under different heat loads and sink temperatures.
- Proper priming, by means of the reservoir.

Concerning the evaporators it can be remarked that:
- Their design has been successfully demonstrated.
- A transport capability of up to 2 x 95 W has been tested.
- 0-g and 1-g heat transfer coefficients have been derived.
- The use and the interaction of two evaporators in parallel have been successfully tested.

Concerning the control reservoir it can be said that:
- The use of a thermal reservoir for the control of the CPL has been successfully demonstrated.
- The capability of the reservoir to prime and re-prime the evaporators has been proven.
- The control of the set-point by managing the loop fluid content through the use of the Peltier cells has correctly operated during the 0-g testing.

Not achieved objectives are:
- Due to the high temperature of the heat sink, the start-up capability at low temperatures has not been tested.
- Due to differential pressure sensor breakdown, the pump pressure across the evaporators has not been assessed.

On the multichannel condensers it is remarked that:
- Experimental results were compared with the predictions obtained with the ESATAN model. Measured flight temperatures of the first condenser match the predicted ones within 1 K. But the predicted temperatures of the second condenser show large deviations from the flight values.
- The heat transfer coefficient values derived from the experimental data turned out to be reasonably constant, however 2000 W/Km^2 higher than predicted. This is

obvious, as the predictions suppose annular flow along the entire condenser, while in reality part of the condensation path is slug flow characterised by higher heat transfer coefficients).

Figure 3 depicts theoretical responses for 0-g and 1-g annular flow, stratified flow and slug flow, flight data and calibration data for 1-g vertical down-flow. It shows that:

- In the low-quality range (slug flow) and in the high-quality range (annular flow) calibration data was found.
- For typical flight conditions (Re < 1000, microgravity), the flow pattern turns out to be slug in the quality range 0 to 0.4. Between 0.7 and 0.95 the pattern turns out to be annular. For the range 0.4 to 0.7 the flow pattern is not clearly defined. It must be churn flow. This shows clearly that the flow pattern transition from slug to annular occurred in TPX I at vapour qualities far above the only value found in literature (0.13). As the control algorithm defined a set point in the quality range 0.4 to 0.75, control exercises could not be executed.
- There is significant difference between 1-g and low-g VQS responses. Terrestrial annular vertical down-flow does not accurately represent actual 0-g annular flow.

In conclusion it can be said that TPX I was successfully flown: many objectives have been met. The design has proven to be a good balance between the consequences of very limited flight opportunities and two conflicting requirements, being:

- At one side the requirement to meet the unknown thermal environment, leading to a design that had to be preferably simple and flexible with respect to environment (location in the payload bay, thermal environments induced by dissipation of neighbours, and STS mission scenario).
- At the other side to aim for as many objectives as possible, leading towards a complex, more risky design.

Theoretical models for two-phase flow & heat transfer have been partly confirmed, others are to be revised and low gravity flow pattern maps are to be created (based on additional flight data).
The viability of 0-g two-phase technology has been proven. But more in-orbit investigations are to be done.

3.2 LHPFX

To demonstrate LHP technology in orbit, the LHPFX (Bienert et al., 1995) has been developed by a team consisting of the US industries Dynatherm (prime) and Hughes, the Center of Space Power/Texas A&M University, the government laboratories NASA Goddard, BMDO, USAF Phillips & Wright Laboratories, and Naval Research Lab, plus (the only non-US participant) NLR. The LHPFX (Fig. 4) was flown a Hitchhiker experiment aboard space shuttle STS-87, from 19-11 to 5-12-1997 (Bienert, et al. 1998). The flight was very successful: 213 operating hours were accumulated during the mission. Tests consisted of numerous start-ups, step power changes from 15 to 400 W, 18 hours low power (20 W) steady state operation, 49 hours high power (200 W) steady state operation, and temperature control tests using a built-in thermostat. Loop operating temperatures ranged from -27 to +66°C. The lowest sink temperature was -34 °C. All flight objectives were met or exceeded: the LHP functioned flawlessly during the entire test programme.

The specific LHP that was tested in this experiment is a direct derivative of the design that will be used with a deployable radiator in a communication satellite. Pertinent parameters of the ammonia LHP are:

- Evaporator: Stainless steel tube (300 mm x 25 mm OD), aluminium saddle sintered nickel 2.2 μm pore wick.
- Transport lines: Stainless steel, 4.5 m long, .45 mm ID.
- Condenser: Flanged aluminium extrusion, 3.7 m long, 4.0 mm ID bonded to a radiator plate.

The LHP is capable to transport more than 800 W in the range -40 to +65 °C. But the available experiment power limited operation in space to about 400 W. The overall conductance is approx. 50 W/K when the condenser is fully active. The experiment was located in a standard, 135 litres NASA Hitchhiker canister. In order to pack the device inside the compact canister, the 4.5 m long vapour and liquid transport lines were coiled. The flanged condenser was bonded to the upper lid of the canister, which served as the thermal radiator. The basic radiator was extended by a “visor”, to maximise the heat rejection capability. Radiator and visor were covered with silver-teflon tape, all other external surfaces were insulated. The Hitchhiker canister was mounted at the starboard side in Bay 6 of the shuttle cargo bay.

The experiment was instrumented with 36 temperature sensors. Kapton heaters on the evaporator allowed the input power to be varied in steps of 12.5 W from zero to 388 W. A small auxiliary heater and a thermostat were on the compensation chamber to evaluate the temperature control capability of the LHP at a fixed setpoint. Another auxiliary heater was on the radiator plate to adjust the initial temperature of the radiator prior to start the LHP. Standard Hitchhiker services for power, data and command of the experiment were used. Command and telemetry interfaces between experiment and Hitchhiker electronics were via a Data Acquisition and Control Unit, an electronics box mounted on the mid-plate between canister and a 12.5 cm extension cylinder. Real time monitoring and command of the experiment was accomplished through ground support equipment from the Hitchhiker control center at NASA Goddard.

The original test plan called for approx. 60 hours experiment operation. The different tests planned were:

- Start-up & power change at low, -50 to -40 °C, medium, -15 to 0 °C and high temperature +20 to +35 °C.
- Quasi-steady state runs at constant high power (200 W).
- Quasi-steady state runs with constant low power (25W).
- Setpoint control for varying input power and sink levels.

All objectives of the original test plan were met. In addition to the planned tests, many extra tests were conducted: the LHP accumulated 213 hours of operating time in microgravity, which means that (as it also follows from the next sections) the flight was very successful.

A large number of start-up tests were conducted. Most start-ups consisted of applying power to the evaporator without any pre-conditioning. A few start-ups were done after the temperature of the compensation chamber had been raised by a few degrees above the initial evaporator temperature. The purpose of this preheating was to ensure that the device had stopped operating. It turned out that this precaution was not necessary because monitoring the temperatures of the

vapour line provided a clear indication when fluid circulation ceased. Anyhow, the two start-up techniques provided valuable insight into the start-up mechanism of a LHP. All start-ups were successful. The original test plan did not include start-ups or operation of the loop heat pipe with an input power of only 12.5 W. It was believed that the device could not reliably operate with such low power. Because of the ease with which the device could be started with 25 W, the 12.5 W level was added during auxiliary tests. The same applies for a start-up with 387.5 W (nominal) also added during the mission.

Power steps from low-to-high and from high-to-low power are important. During power-down steps, liquid must rapidly move from the compensation chamber into the condenser. This must be accomplished by the secondary wick between evaporator and compensation chamber. Power-down steps are therefore an important test of the capability of the secondary wick. All power cycle tests were completely successful. Additional power cycle tests were conducted during which the evaporator power was held constant for two hours at each level.

Two types of steady tests were conducted: one at high power (200 W), one at low power (25 W). The higher power was selected as the maximum power that can be rejected by the radiator without exceeding safe operating temperature limits. The lower power was believed to be the lowest value, with which the device reliably operates.

In the orbiter bay-to-wake attitude the radiator is exposed to sunlight during part of the orbit and sees deep space during the rest. Hence the sink temperature varies periodically in the 90 minutes orbit. The evaporator temperature does not copy these variations because the LHP functions as a variable conductance device.

The LHP functions as a variable conductance device as long as full utilisation of the condenser is not required to reject the applied heat load. In this regime, the active condenser length is self-adjusting in such a manner that the evaporator temperature remains nearly constant. This behaviour was clearly observed during low power operation. An example of this passive temperature control is the low power steady state test described before.

Active temperature control can be maintaining the temperature of the compensation chamber constant (and with it the vapour pressure). A 25 W heater and a thermostat were attached to the compensation chamber for this purpose. The thermostat had a setpoint of 35 to 38 °C. After activating the evaporator heater, the loop did not start until the evaporator temperature exceeded the set point. The evaporator temperature then cycled in tandem with the compensation chamber. When the evaporator power was raised to 100 W, its temperature rose slightly, but the vapour temperature continued to follow the oscillations of the compensation chamber. Closer temperature control could be achieved with a "smarter" controller, e.g. by using a computer algorithm to control the compensation chamber temperature. An attempt was made to simulate a "smarter" controller by controlling the temperature manually. This approach reduced the control band on the evaporator from 6 °C to less than 2 °C. This data need further analysis because this test was interrupted several times by loss of telemetry and commands. Both temperature control tests also showed the expected loss of temperature control capability at higher powers (>200 W) since the entire condenser is then needed to reject the heat.

3.3 TPX II

To usefully and economically fill the time gap between TPX and future full-scale CPL and LHP flights, TPX II (an updated TPX I) was manifested built and flown as Get Away Special G467 on STS-95, October 1998. TPX II (Delil et al., 1997) used many TPX I parts, while TPX I components, that functioned improperly or non-optimally, were replaced or refurbished. Other components were replaced by advanced ones, developed since the TPX I start (evaporators, three-way valve). The number of temperature sensors was doubled. It was accounted for the lessons learned in TPX I. The updated scenario included completion of experiments not completed in TPX I and allowed testing of earth observation spacecraft type (ATLID like) applications (Dunbar, 1996), with thermally unbalanced parallel condensers, simulating spacecraft radiators exposed to differently phased radiation environments.

The TPX II schematic is shown in figure 1b. The main changes, with respect to TPX I, are:

- New evaporator designs (with sintered nickel wicks to yield a high pumping power), connected to the reservoir by capillary links (to guarantee proper start-ups).
- A more accurately controllable bypass valve and tuned vapour bypass line flow resistance.
- An updated position of the reservoir-loop connection.
- Condensers in parallel, instead in series, to simulate unbalanced sink temperatures, typical for earth observation spacecraft applications (Dunbar, 1996).
- Refurbished LFM and new Differential Pressure Sensor (DPS) and Absolute Pressure Sensor (APS).
- A larger number of temperature sensors (78).
- An updated flight scenario.

To reduce costs and to meet time constraints, TPX II design, manufacture and assembly is entirely based on the TPX I approach. The configuration comparable with the TPX I configuration. The DAC system is the TPX I system, the battery is a battery like in TPX I. The evaporators contain 2 μm sintered nickel wicks (void fraction 0.71 and permeability $5*10^{-14}$ m^2). Nominal power is 200 W at 250 mm tilt. The capillary pumping pressure is up to 38000 Pa. The control reservoir is like the TPX I control reservoir, but with capillary links to the evaporators to guarantee proper start-up. Another innovative aspect of TPX II is the configuration with two parallel condensers. One is equipped with a 30 W electrical heater to create unbalanced heat sinks. The condensers are aluminium rectangular grooved heat pipe profiles (15 x 15 x 235 mm^3), with welded end caps. The end cap at the outlet of a condenser was designed to restrict the vapour flow leaving the condenser. The condensers dissipations is at least 100 W (nominal) for an overall thermal resistance of 0.29 W/K. To achieve a constant conductance of 7500 W/m^2K, a teflon filler (thickness 0.03 mm) is between the condensers and the heat sink. The VQS was used in TPX I (refurbished and re-calibrated). Vapour control exercises are using the VQS and a novel control valve of Bradford. Like in TPX I, a DPS is arranged in parallel to the evaporators.

The new DPS allows differential pressure measurements from 0 to 10000 Pa with an accuracy of ± 1% FS within a temperature range from 253 to 353 K. The loop pressure is measured by an ENTRAN Absolute Pressure Sensor: 70 Bar max., accuracy ± 0.25% FS. As in TPX I, two INTEK LFM are in the loop. Finally it is remarked that a completely new NASA safety policy led to delays, in particular in the loop assembly.

After experiment retrieval it turned out that there were no flight data, as TPX II was not switched on during flight, because of a software failure caused by an EPROM with a misspelled checksum. Post-flight tests, executed after inserting a correct flight EPROM, proved that the experiment performed excellently, like it did before launch. Therefore it was decided to re-fly the experiment as soon as there is a flight opportunity.

4. TWO-PHASE SYSTEM COMPONENTS

Other components developed for two-phase systems (with NLR involvement) will be discussed in the next.

4.1 Rotatable Radial Thermal Joint

Recalling earlier discussions (Delil, 1987), it is remarked that dedicated heat pipe radiators will be used to reject waste heat into space. Such a radiator, stowed during launch, will be deployed in orbit. The radiator may even be chosen to be steerable for maximum performance, hence minimum radiator size/mass. In such radiator systems, the coupling to the central (two-phase) loop or heat pipe has to incorporate a rotatable/flexible thermal joint. Drivers for the design of such joints are low thermal resistance, hence limited temperature drop across the joint, and small deployment/retraction or steering torque. A quantitative discussion on joint concepts identified the rotatable radial heat pipe as a promising solution for steerable radiators (Delil, 1987). Figure 5 shows a schematic of a rotatable radial heat pipe. An essential component is the wick to provide the capillary head to return the condensate from condenser to evaporator and to distribute the liquid properly over the evaporator surface. Therefore the fine gauze wick structure should be uniformly fixed to the evaporator surface (inner tube outer surface). In this way burnout, caused by blockage due to vapour bubbles generated, is prevented. Since the outer tube must be rotatable with respect to the inner tube there must be a clearance between porous structure and tube wall. This clearance is located at the condenser, the less critical side of the heat pipe, where the condensate has to be collected only (relatively easy, especially for a slightly overfilled heat pipe). An accurate design combines proper condensate collection and transport, hence good heat pipe performance, and low rotation torque, hence long lifetime for a steerable radiator. It is obvious that the end caps of a rotatable radial heat pipe must be leak-tight. This problem must be solved using appropriate seals. The thermal performance of a radial heat pipe is hard to predict. A rough estimate follows from flat plate vapour chamber data: a heat transfer coefficient of 4000 W/m^2. K, for methanol as working fluid, between 250 and 305 K. For a radial joint with an external diameter of 40 mm, this means a conductance of 500 W/K per meter joint length.

A simple 10 cm long test specimen (Fig. 6a) has been manufactured to prove the feasibility of the concept (Delil et al., 1997). It simulates the realistic configuration (Fig. 6b), and consists of a 10/12 mm inner tube, cooled by liquid flow, simulating the heat pipe. A 13/15 mm outer tube, heated by a heater simulating the heat source, a condensing two-phase mixture. A rotatable section (ball valve) allows outer and inner tube to rotate with respect to each other. 0.5 mm clearance between the tubes contains wick simulating metal gauze. Working fluid is R114.

Figure 7 shows the results of a test to determine the optimum working fluid content. Starting with pure liquid, the temperature drop across the joint is about 13 K. By stepwise blow-off R114 this temperature drop is reduced to 7 K at the optimum mixture quality. Continuing blow-off increases the temperature drop up to 26 K (pure vapour conduction/solid conduction of the gauze). The optimum joint conductance is 3 W/K for this 0.1 m long, 13 mm OD R114 joint, or 600 W/K for the mentioned 4 cm OD, 1 m long methanol filled joint, or 1500 W/K with ammonia as working fluid.

Figure 8 shows the optimally filled joint performance, during rotation (at 17 revolutions/hr) and in non-rotating periods, for different power values (45, 35 and 20 W). The figure confirms the mentioned joint conductance value, both for the rotating and non-rotating case. This conductance, showing to be more stable in the non-rotating case, increases slightly with power (temperature).

In summary: The concept is feasible, the joint did not leak and the performance figures are promising. Seal improvement and use of a buffer volume (also filled with working fluid at approximately the same, heat pipe, temperature) are expected to lead to the realisation of a mature long lifetime rotatable radial heat pipe joint.

4.2 Condensers

Efficient Low Pressure Drop condensers/radiators are crucial for two-phase systems. Two radiator solutions can be distinguished. In a direct condensing radiator is the condenser attached to the radiator, radiating condensation heat to space. In a hybrid radiator is the condenser not an integrated part of the radiator (condensation heat is transported from condenser via central heat pipe to heat pipes distributing the heat over the radiator).

Two direct condensing radiators have been designed and manufactured for the ATLID Laser Head Thermal Control Breadboard (Fig. 9), developed for ESA by MSS-UK (prime), NLR and Bradford (Dunbar, 1996). They are configured to represent the allowable areas for the ATLID instrument on the Polar Platform. One radiator, 1.05 m high by 1.0 m wide (radiator A), is fixed to the instrument base plate and supported by struts. The other radiator (B), 0.8 m high and 1.45 m wide, is deployable and fixed only along its edge by cantilever support beams. The struts for radiator A are constructed from filament wound carbon fibre tubes with aluminium end fittings. The cantilever beams of radiator B are 100 mm deep to provide adequate stiffness. The radiators are too small to reject the heat load in steady state conditions. They are only just capable of meeting the heat rejection requirements when a full orbital cycle is considered. The radiator B deployable design includes a unique torsion/helical bending configuration to

minimise pipe strain and allow multiple repetition of the deployment. Although the instrument requires deployment only for ground access, the design is equally suitable for flight deployment. The radiator surfaces would for flight be covered with advanced glass optical solar reflectors to give low beginning and end of life solar absorptivities. For the breadboard tests sunlight has been simulated by altering heat sink temperatures, and the radiators are simply black painted. The radiators are constructed from extruded aluminium profiles rivetted together to form a continuous surface. Each profile section contains one 2 mm ID condensing pipe, clamped into good thermal contact with a channel in the extrusion. Isolators in each liquid line and one at the liquid header outlet ensure even vapour distribution and prevent differential dry-out. The rivetted construction provides stiffness in two axes, the other is stiffened by adding a beam crossing all profiles.

The ATLID test programme conclusions (Dunbar 1996) can be summarised by:

- The two-phase system is treated as just another thermal tool, able conform to installation, accommodation and structural requirements set by the overall instrument.
- The system has successfully completed severe sine and random vibration tests to qualification levels.
- The deployable radiator concept has been demonstrated.
- The tests demonstrated that the breadboard meets or exceeds nearly all performance requirements. In particular the principal requirement to maintain the laser diode interface to within 1 °C of the nominal temperature during simulated low earth orbits was met with a significant margin. Due to restrictions on radiator area the end of life heat rejection performance only just meets the requirements. Extra margin is recommended.
- Modifications will be necessary if the 125 Hz first radiator frequency is to be met for actual flight units, but these were identified and are not considered critical.

For ESA, a high efficiency, low pressure drop condenser (Fig. 10) for a hybrid (heat pipe) radiator has been successfully developed and brought up to pre-qualification level, by NLR (prime), Bradford and DASA (Delil et al., 1996). This condenser has been subjected to tests under “in-orbit” conditions: vapour temperature 263 - 313 K, for a condensed power up to 300 W. The tested hybrid condenser design consists of a concentric tube around a liquid cooled inner tube, simulating the heat pipe. The vapour, entering the condenser, is uniformly distributed by a cone. The condensing part is an annulus with ID 25 mm and OD 28 mm, hence a gap width 1.5 mm. Six wires with a diameter of 1.5 mm subdivide the annulus into six parts. The wires are coiled around the central tube, leading to helical condensation channels, providing a swirl to improve performance.

The tests proved the quality of the design, being a good compromise between high-efficient thermal performance and low pressure drop (Fig. 11): for 300 W, a temperature drop below 7.5 K at a pressure drop below 400 Pa (the latter can be reduced by increasing the number of condenser outlet vapour stops). The tests proved that there is no significant difference in performance for vertical and horizontal orientation. The condenser design satisfied all other requirements. Three of these condensers in series, with 25 mm OD central heat pipes, are part of ESA’s Capillary-pumped Loop Engineering Model CLEM, currently studied by MMS-UK (prime), Bradford, MMS-F and NLR.

5. DESIGN SUPPORTING THEORETICAL WORK

Supporting theoretical work, the modelling and scaling of two-phase heat transport systems (Delil, 1991 & 1998), is done:

- For a better understanding of two-phase flow and heat transfer phenomena.
- To provide means to compare and generalise data.
- To develop a useful tool to design two-phase systems and components, to save money and to reduce costs.

Examples of the scaling of two-phase flow and heat transfer can be found in the power and in the process industry. The scaling of physical dimensions is of major interest in the process industry: large-scale industrial systems are studied by reduced scale laboratory systems. The scaling of the working fluid is of principal interest in the power industry, where large industrial systems characterised by high heat fluxes, temperatures, and pressures, are translated in full size systems, operating at lower temperature, heat flux and pressure levels (e.g. scaling a high pressure water-steam system by a low pressure refrigerant system of the same geometry).

Main goal of scaling space-related two-phase heat transport systems is the development of reliable spacecraft systems of which the proper low-gravity performance can be predicted using experimental data of scale models on earth. Scaling of spacecraft systems can be useful also:

- For in-orbit technology demonstration: the performance of spacecraft heat transport systems can be predicted using outcomes of in-orbit experiments on models with reduced geometry or different working fluid.
- To define in-orbit experiments for isolating typical phenomena to be investigated, e.g. excluding of gravity-induced disturbing buoyancy effects on alloy melting, diffusion and crystal growth, for a better understanding of the physical phenomena.

The magnitude of the gravitational scaling varies with the objectives, from:

- 1 to 10^{-6} g (random direction) for the terrestrial scaling of orbiting spacecraft.
- 1 to 0.16 g for Moon, to 0.4 g for Mars base systems.
- 10^{-2} or 10^{-6} g to 1 g for isolating gravity-induced disturbances on physical phenomena investigated.
- Low-g to another or the same low-g level for in orbit demonstration (in low-g aircraft or sounding rockets).

One-g is not the upper limit in gravitational scaling: higher g-values can be obtained during special aircraft trajectories, or by rotation e.g. the centrifugal scaling of isothermal separated gas-liquid flow in a tube, fast rotating a tube around an external axis (Geraets, 1986).

Unfortunately, even in single-phase systems scaling is all except simple, as flow and heat transfer are equivalent in model and original (prototype) system only if the corresponding velocity, temperature and pressure fields are identical. Dimensionless numbers can be derived either from the conservation equations for mass, momentum and energy or from similarity considerations, based on dimension analysis. The above identity of

velocity, temperature and pressure fields is obtained if all dimensionless numbers are equal in model and prototype.

Scaling two-phase systems is far more complicated as:
- In addition to the aforementioned fields, the spatial distribution (void and flow pattern) is to be considered.
- Geometric scaling often has no sense if characteristic sizes, e.g. bubble diameter and surface roughness, are almost independent of system dimensions.
- There is a proportion problem, arising from two-phase flow and boiling heat transfer high power density levels.

5.1 Similarity Considerations/Dimension Analysis

Similarity considerations, discussed in detail in Delil, 1991 & 1998, led to the identification of 18 dimensionless numbers (π-numbers) which are relevant for thermal gravitational scaling of two-phase loops. These 18 π-numbers are listed in table 1, showing the relevance of π-numbers in the various loop sections.

As said before, perfect similitude between model and prototype is obtained if all dimensionless numbers are identical in prototype and model. Then there is perfect similitude and only then the scaling is perfect. It is evident that perfect scaling is not possible in the case of two-phase flow and heat transfer: the phenomena are too complex, the number of important parameters or π-numbers is too large. Fortunately also imperfect (distorted) scaling can give useful results. Therefore a careful estimation of the relative magnitudes of the different effects is required. Effects, identified to be of minor importance in two-phase systems are Mach number in incompressible flow in liquid lines, and Froude number (gravity) in pure vapour flow.

Finally it is remarked that in scaling a two-phase heat transport system:
- Geometric distortion is not permitted to study boundary layer effects and boiling, as identity of surface roughness in prototype and model is to be guaranteed.
- Geometrical distortion is a must when the length scaling leads to not practically small (capillary) conduits in the model, in which the flow phenomena basically differ from flow in the full size prototype.

Sometimes it is more convenient to replace quality X by the volumetric vapour (void) fraction α, according to:

$$(1 - \alpha)/\alpha = S\,(\rho_v / \rho_l)\,/\,(1- X)/X. \qquad (1)$$

It is clear that the set of π-numbers presented is rather arbitrary one, e.g. several numbers contain only liquid properties. These numbers can be easily transferred into vapour properties containing numbers using π_6, π_7 and π_8. Similarly π_1 can be used to interchange characteristic length (e.g. duct length, bend curvature radius) and a characteristic diameter (e.g. duct diameter, hydraulic diameter, but if desired also surface roughness/bubble diameter). Sometimes it will even be convenient to simultaneously consider two geometric π_1 numbers: one for the overall channel (channel diameter versus length or bend radius), the other pertaining to other parameters (the ratio surface roughness and bubble diameter to investigate boiling heat transfer, or the ratio of surface roughness and channel diameter to study friction pressure drop).

Generally speaking, combinations of π-numbers are chosen such that they optimally suit the problem under investigation. Typical examples are:
- The Morton number

$$\pi_{15} = Mo_l = Re_l^{\,4}\,Fr_l / We^3 = \rho_l\ \sigma^3 / g\ \mu_l^{\,4} \qquad (2)$$

being especially useful for scaling two-phase flow with respect to gravity (since it contains, apart from gravity, only liquid properties and surface tension).
- The Mach number

$$\pi_{16} = Ma = v/(\partial p/\partial \rho)^{1/2}, \qquad (3)$$

when compressibility effects are important (e.g. choking strongly depends on homogeneous two-phase quality).
- The boiling number

$$\pi_{14} = Bo = Q / \dot{m}\, h_{lv} = \Delta H / h_{lv}\ , \qquad (4)$$

Q is the power fed to the boiling liquid. This number appears in the expression for the dimensionless enthalpy at any z in a line heated from outside

$$\Delta H(z) / h_{lv} = \Delta H_{in} / h_{lv} + \pi\, D\, z\, q / \dot{m}\, h_{lv.} \qquad (5)$$

q is heat flux. For sub-cooled or heated liquid it is:

$$\pi_{14} = Q / \dot{m}\ Cp_l\ \Delta T, \qquad (6)$$

ΔT is the temperature drop. This implies that, if the dimensionless entrance enthalpies are equal for different fluids in similar geometry, equal boiling numbers ensure equal dimensionless enthalpy at similar axial locations. In thermodynamic equilibrium it means equal quality at similar locations and similar sub-cooling/boiling length.
- The condensation number

$$\pi_{17} = (h / k_l)\ (\mu_l^{\,2} / g\ \rho_l^{\,2})^{1/3}, \qquad (7)$$

h being the local heat transfer coefficient.
- The vertical wall condensation number

$$\pi_{18} = L^3 \rho_l^{\,2}\, g\, h_{lv} / \mu_l\, k_l\, (T- T_o). \qquad (8)$$

T_0 is the local sink, T the local saturation temperature.

A first step in a practical approach to scale two-phase heat transport systems is the identification of the important physical phenomena, in order to obtain the π-numbers for which identity in prototype and model must be required to realise perfect scaling according to Buckingham´s theorem. Distortion will be permitted for π-numbers pertaining to phenomena considered less important. That the important phenomena and the relevant π-numbers will be different in different parts of a system is obvious. Table 1 shows the relevance (• is relevant) of the π-numbers in the various loop sections.

For refrigerants like ammonia and R114, forced convection heat transfer overrules conduction completely, hence π_{10} π_{11} and π_{12} are not critical in gravitational scaling. π_{16} can be neglected also, since the system maximum power level and line diameters correspond with

flow velocities far below the sonic velocity in all parts of the systems including the two-phase sections.

Considering π_3/π_5, it can be remarked that inertia overrules buoyancy not only in pure vapour flow or in a low gravity environment, but also for horizontal liquid sections on earth ($\nu \rightarrow \pi/2$). This implies that there is π-number identity for these sections in low-g prototype and in a terrestrial model, for a horizontal arrangement of these sections. Also it can be remarked that, in the porous (liquid) part of a capillary evaporator, surface tension forces ($2\sigma/D_p$) are dominant over inertia ($\pi_9 \rightarrow 0$), and consequently the evaporator exit quality will approach 1 (pure vapour). This means that gravity is not important for the vapour part of the evaporator and for the vapour line connecting evaporator and condenser.

Important conclusions can be drawn now:

- The condensers and, in the mechanically pumped system also the two-phase lines, are crucial in scaling with respect to gravity. They determine the conditions for the evaporators and single-phase sections. The latter can be scaled in the classical way presented in text books.
- In the adiabatic two-phase lines (in the mechanically pumped mode) under low-gravity conditions only shear forces are expected to cause the separation of the phases in the high-quality (above say 0.8) mixture, leading to pure annular flow (a fast moving vapour in the core and a by frictional drag induced slowly moving liquid annulus at the inner line wall) for the lower flow rates. For increasing power, hence flow rate, the slip factor increases, introducing waves on liquid-vapour interface and entrainment of liquid in the vapour: so-called wavy annular/ mist flow. Similar flow pattern behaviour can be predicted for vertical downward flow on earth, as it easily can be derived from the flow pattern map for downward two-phase flow (Fig. 12), taken from Oshinowo & Charles, 1974), in which water properties at 20 ˚C must be used to determine the scale of the abcissa. The Froude number for two-phase flow used in this figure is defined as:

$$Fr_{tp} = (16\,\dot{m}^2/\pi^2 D^5 g)[X^2/\rho_v^2 + (1-X)^2/\rho_l^2] \,. \qquad (9)$$

Comparing low-g and vertical down-ward terrestrial flow one has to correct the latter for the reduction of the slip factor by the gravity forces assisting the down-flowing liquid layer. Anyhow, vertical down-flow is the preferred two-phase line orientation in the terrestrial model because of the axial-symmetric flow pattern. A similar conclusion can be drawn for the straight tube condenser. Recalling figure 12, it is remarked that in these condensers the flow will change from wavy/annular/mist to pure liquid flow, passing different flow patterns, depending on the condensation path.

5.2 Scaling Examples and Experiments

Consequences of scaling are elucidated by the figures 13 and 14, showing the temperature dependence of g.Mo$_l$ or $\rho_l\sigma^3/\mu_l^4$ and σ/ρ_l, a constituent of $(We/Fr)^{½}$.

In case of scaling at the same gravity level it can be seen in figure 13, that the value $\rho_l\sigma^3/\mu_l^4 = 2*10^{12}$ m/s^2, can be realised by seven systems, i.e. a 115°C ammonia, 115°C methanol, 35°C water, 180°C propanol, 235°C propanol, 250°C thermex and a 350°C thermex system. Requiring, in addition to Morton Number identity, also the identity in $(We/Fr)^{½}$, in other words $D/(\sigma/\rho_l)^{½}$, the length scales of the seven systems derived from the corresponding (σ/ρ_l)-values in figure 14, turn out to be proportional to each other with ratios 2.5: 4.5: 8.4: 4.2: 3.0: 5.0: 3.6. Hence the maximum scaling ratio obtainable equals $8.4/2.5 \approx 3$, indicating that geometry scaling at the same gravity level can cover only a limited range.

In addition, the scaling of high pressure (say 110 °C) ammonia system parts by low pressure (say -50 °C) ammonia system parts might be attractive for safety reasons or to reduce the impact of earth gravity in vertical two-phase sections. In a similarly manner as the above, one can straightforwardly derive from figure 14, that the length scale ratio between high-pressure prototype and the low-pressure model (characterised by $\rho_l\,\sigma^3/\mu^4_l = 2.10^{12}$ m/s^2) is $L_p/L_m = [(\sigma/\rho_l)_p/(\sigma/\rho_l)_m]^{1/2} \approx 0.4$. For ammonia such a scaling can be attractive only for sections without heat transfer, since otherwise it will certainly lead to unacceptable high power levels in the model system evaporators and condensers.

Figure 13 shows that the scaling with respect to gravity is restricted to say two decades, if the fluid in prototype and model is the same, e.g. a 10^{-2} g, 80 °C, thermex prototype can be scaled by a 300 °C thermex model on earth. The length scaling is $L_p/L_m = D_p/D_m = (g_m/g_p)^{½}\,(\sigma/\rho_l)_p^{½}/(\sigma/\rho_l)_m^{½} \approx 14$.

More interesting is fluid to fluid scaling: e.g. alkali metal terrestrial prototypes can be scaled by various model systems in space, a 400°C mercury prototype:

- At 10^{-2} g, by a 35°C ammonia model ($L_m/L_p \approx 11$) or 80°C water model ($L_m/L_p \approx 14$).
- At 10^{-4} g, by a methanol model at 35°C ($L_m/L_p \approx 95$), a 130°C thermex ($L_m/L_p \approx 100$), a 30°C R114 ($L_m/L_p \approx 45$).

It is obvious that space-oriented mercury systems must be scaled on by other fluid systems in centrifuges on earth. In addition it can be said that a 25°C R114 prototype at 10^{-2} g can be scaled by a 25°C, 1 g ammonia model ($L_p/L_m \approx 5$), important for the ESA developments discussed next.

To support ESA two-phase activities (TPX I and TPHTS), experiments had to be carried out using the NLR two-phase test rig. This ammonia rig, having approx. the same line diameter as the TPX I loop, has been used for:

- Testing and calibration of TPX I & II and components.
- The scaling of low-g adiabatic and condensing flow as discussed in the following sections: terrestrial, low temperature, vertical down-flow minimises the impact of gravity, hence simulates low-gravity conditions the best.

In addition it is recalled that the full size low-gravity (< 10^{-2} g) mechanically-pumped R114 ESA TPHTS can be adequately scaled by the above ammonia test rig, since:

- The, say 10^{-2} - 10^{-3} g, R114 prototype and the terrestrial ammonia model have approx. identical Morton number.
- This fluid to fluid scaling leads towards a corresponding length scaling $D_p/D_m = (g_m/g_p)^{½} * (\sigma/\rho_l)^{½}_p / (\sigma/\rho_l)^{½}_m \approx 4.5$ to 6.5, which is in agreement with the ratio of the actual diameters, 21 mm for the R114 space-oriented prototype and 4.93 mm for the terrestrial ammonia model.

In summary it can be said that the scaling of two-

phase heat transport systems is very complicated. Only distorted scaling offers some possibilities, especially when not the entire loop but only loop sections are involved. Scaling with respect to gravity is hardly discussed in literature. Some possibilities can be identified, though for typical and very limited conditions only. The mechanically pumped NLR two-phase ammonia test rig offers: Some opportunities to scale a TPX I ammonia loop and a very promising application: the terrestrial scaling of a ESA mechanically pumped TPHTS (R114) flight unit.

5.3 Modelling Two-Phase Pressure Drops

An important quantity to be measured during two-phase flow experiments is the pressure drop in adiabatic sections and in condensers: sections considered crucial for two-phase system modelling and scaling. Therefore we will concentrate in the following on the modelling of pressure drops in condensing and adiabatic flow. We will restrict the discussion to straight tubes.

The total local (z-dependent) pressure gradient for annular two-phase flow is the sum of the contributions of friction, momentum and gravity:

$$(dp(z)/dz)_t = (dp(z)/dz)_f + (dp(z)/dz)_m + (dp(z)/dz)_g \qquad (10)$$

Following Delil (1991 & 1992) and Soliman (1968), an elaborate publication on the subject, one obtains for the contribution of friction (deleting the z-dependence to shorten the notation):

$$(dp/dz)_f = - (32\dot{m}^2/\pi^2\rho_v D^5)(0.045/Re_v^{0.2})[X^{1.8} + \\ + 5.7(\mu_l/\mu_v)^{0.0523}(1-X)^{0.47}X^{1.33}(\rho_v/\rho_l)^{0.261} + \\ + 8.1(\mu_l/\mu_v)^{0.105}(1-X)^{0.94}X^{0.86}(\rho_v/\rho_l)^{0.522}]. \qquad (11)$$

X is the local quality X(z), Re_v is the Reynolds number

$$Re_v = 4\,\dot{m}/\pi\, D\, \mu_v\,. \qquad (12)$$

The fluid properties μ_l, μ_v, ρ_l and ρ_v are assumed to be independent of z, as they depend only on the mixture temperature, usually being almost constant in adiabatic and condensing sections.

The momentum constituent can be written as

$$(dp/dz)_m = - (16\dot{m}^2/\pi^2D^4)\{[2X(1-\alpha)/\rho_v\alpha^2 - \beta(1-X)/\rho_l\alpha + \\ + (1-\beta)(1-X)/\rho_l(1-\alpha) + (1-X)/\rho_l(1-\alpha)](dX/dz) + \\ - [X^2(1-\alpha)/\rho_v\alpha^3 + (1-X)^2/\rho_l(1-\alpha)^2](d\alpha/dz)\}. \qquad (13)$$

α is the z-dependent local void fraction $\alpha(z)$. $\beta = 2$ for laminar liquid flow, $\beta = 1.25$ for turbulent flow.
The gravity constituent is

$$(dp/dz)_g = (1-\alpha)(\rho_l-\rho_v)g\cos\nu. \qquad (14)$$

$g \rightarrow 0$ for microgravity conditions and $g.\cos\nu$ equals 9.8 m/s^2 for vertical down-flow on Earth, 3.74 m/s^2 for vertical down-flow on Mars and 1.62 m/s^2 on the Moon.
α is eliminated in eq. (13) and (14) by inserting eq. (1).

The slip factor S is to be specified. The principle of minimum entropy production (Zivi, 1964) leads to.

$$S = [(1+1.5Z)(\rho_l/\rho_v)]^{1/3} \qquad (15)$$

for annular flow, in which the constant Z (according to experiments) is above 1 and below 2, and

$$S = \{(\rho_l/\rho_v)[1+Z'(\rho_v/\rho_l)(1-X)/X]/[1+Z'(1-X)/X]\}^{1/3} \qquad (16)$$

for real annular-mist flow, that is annular flow with a mass fraction Z' of liquid droplets entrained in the vapour core. Z' is between 0 for zero entrainment and 1 for complete entrainment. For the limiting cases Z and $Z' \rightarrow 0$, eqs. (15) and (16) become:

$$S = (\rho_l/\rho_v)^{1/3} \qquad (17)$$

The latter relation, representing ideal annular flow, will be used here for reasons of simplicity and since it allows a comparison with the results of calculations found in literature. The influence of $Z \neq 0$ and $Z' \neq 0$ is interesting for future investigations.
Insertion of eq. (17) into eq. (1) and (11, 13, 14), yields:

$$(dp/dz)_m = - (32\dot{m}^2/\pi^2\rho_v D^5)(D/2)(dX/dz) * \\ * [2(1-X)(\rho_v/\rho_l)^{2/3} + 2(2X-3+1/X)(\rho_v/\rho_l)^{4/3} + \\ + (2X-1-\beta X)(\rho_v/\rho_l)^{1/3} + (2\beta - \beta X - \beta/X)(\rho_v/\rho_l)^{5/3} + \\ + 2(1-X-\beta+\beta X)(\rho_v/\rho_l)]. \qquad (18)$$

$$(dp/dz)_g = (32\dot{m}^2/\pi^2\rho_v D^5)\{1-[1+(\rho_v/\rho_l)^{2/3}(1-X)/X]^{-1}\} * \\ * [\pi^2 D^5 g\cos\nu(\rho_l-\rho_v)\rho_v/32\dot{m}^2]. \qquad (19)$$

To solve eqs. (11, 18, 19) an extra relation is necessary, defining the z-dependence of X. A relation often used

$$dX/dz = -X_{entrance}/L_c \qquad (20)$$

(L_c being the condensation length), means uniform heat removal (hence a linear decrease of vapour quality along the duct), which may be unrealistic. It is better to use

$$\dot{m}\, h_{lv}(dX/dz) = - h\pi D[T(z)-T_s]\ , \qquad (21)$$

relating local quality and heat transfer. h is the local heat transfer coefficient h(z), for which one can write

$$h = 0.018\,(k_l\,\rho_l^{1/2}/\mu_l)\,Pr_l^{0.65}\,|-(dp/dz)_l|^{1/2}\,D^{1/2} \qquad (22)$$

The latter equation has been derived, by Soliman et al. (1968), assuming that the major thermal resistance exists in a laminar sub-layer of the turbulent condensate film.
As already mentioned the two-phase flow path is almost isothermal, which implies constant temperature drop $T(z) - T_s$ (for constant sink temperature T_s), constant fluid properties and a constant Prandtl number, defined by

$$Pr_l = (Cp_l\,\mu_l)/\,k_l. \qquad (23)$$

The total condensation pressure drop is

$$\Delta p_t = \int_0^{L_c} (dp/dz)_t dz. \quad (24)$$

Eqs. (10, 11, 18, 19, 21) and eq. (22) can be combined, yielding an implicit non-linear differential equation in the variable X(z), which can be rewritten into a solvable standard form for differential/ algebraic equations

$$F(dX/dz, X) = 0. \quad (25)$$

Ten Dam & Van den Berg (1992) discuss mathematical details and numerical solution methods of this differential-algebraic equation.

5.4 Quantitative Examples

Comparing adiabatic flow pressure gradient constituents at two temperatures, calculated according to the equations presented above, proves that the gravity constituent is overruled by the others at low temperature (Delil, 1991). This means that low-g behaviour can be investigated by terrestrial tests at low temperature. Figure 15 shows that the calculations for adiabatic annular flow pressure gradients confirm (the pressure drops over an adiabatic section, determined experimentally during low-g aircraft flights with a R114 system (Chen et al., 1991).

Modelling and calculations have been extended from adiabatic towards condensing flow in a straight condenser duct (Delil, 1992) to investigate the impact of gravity level on the duct length required to achieve complete condensation. This impact, which has been reported to lead to duct lengths up to more than one order of magnitude larger for zero gravity as compared to horizontal orientation in Earth gravity (Da Riva & Sanz, 1991), has been assessed (Delil, 1992) for various mass flow rates, duct diameters and thermal (loading) conditions, for two working fluids i.e. ammonia (working fluid for the Space Station, for capillary pumped two-phase systems and for TPX) and R114 (working fluid of the ESA TPHTS).

A summary of results of calculations carried out for ammonia, the most promising working fluid for future two-phase systems, is presented next.

To compare the results of the calculations with data from literature, the condenser defined by Da Riva & Sanz, 1991, was chosen as the baseline (main characteristics are power Q = 1000 W, line diameter D = 16.1 mm, ammonia temperature T = 300 K and a temperature drop to sink ΔT = 10 K. The other parameter values are listed below.

T	(K)	300	243	333
h_{lv}	(J/kg)	$1.16*10^6$	$1.36*10^6$	$1.00*10^6$
$\dot{m}$	(kg/s)	$8.64*10^{-4}$	$7.36*10^{-4}$	$9.98*10^{-4}$
μ_l	(Pa.s)	$1.40*10^{-4}$	$2.47*10^{-4}$	$0.94*10^{-4}$
μ_l/μ_v	(-)	12.30	30.66	8.54
ρ_l	(kg/m^3)	600	678	545
ρ_l/ρ_v	(-)	72.46	652.4	26.6
k_l	(W/m.K)	0.465	0.582	0.394
Pr	(-)	1.42	1.90	1.25

Gravity levels considered are zero gravity g=0, Earth gravity (1-g) g=9.8 m/s^2, Mars gravity g=3.74 m/s^2, Moon gravity g=1.62 m/s^2, and 2-g macro-gravity level 19.6 m/s^2. Illustrative results of calculations are discussed next.

Figure 16 shows the vapour quality X along the condensation path (as a function of non-dimensional condensation length z/D) for all gravity levels mentioned, including the curves of Da Riva & Sanz, 1991, for zero-g and horizontal condensation on earth. The curves start at entrance quality 0.96 for which annular flow, assumed in the modelling, is expected to be established. From this figure it can be concluded that:

- The length required for full condensation strongly increases with decreasing gravity: 0-g condensation length is roughly 10 times the terrestrial one.
- The data presented by Da Riva & Sanz, 1991, can be considered as extremes: a horizontal condensation length of say 50% of the terrestrial downflow length (induced by the stratified flow pattern that enhances the transfer area and heat transfer coefficient) and higher zero-g predictions (induced by the equation for the heat transfer coefficient used, being different from the model presented here).

To assess the impact of the fluid saturation temperature on condensation performance, similar curves have been calculated for two other temperatures, 243 K and 333 K and the above parameter values (Delil, 1992). The calculations show that the full condensation length increases with the temperature for zero gravity conditions, but decreases with temperature for the other gravity levels. This implies that the differences between Earth gravity outcomes and micro-g outcomes decrease with decreasing temperature, confirming the statement already made: the effect of gravity is reduced under lower temperature vertical down-flow conditions.

Calculation of the vapour quality distribution along the 16.1 mm reference duct for condensing ammonia (at 300 K) under Earth gravity and 0-g conditions, for power levels from 0.5 kW up to 25 kW, yielded (Delil, 1992):

- A factor 50 in power, 25 kW down to 500 W, corresponds in a zero gravity environment to a relatively minor reduction in full condensation length, i.e. from say 600 D to 400 D (from 9.5 to 6.5 m).
- Under Earth gravity conditions, power and full condensation length are strongly interrelated: from L_c = 554 D at 25 kW to only 19 D at 500 W.
- The gravity dependence of the full condensation length decreases with increasing power, until the differences vanish at roughly 1 MW condenser choking conditions. The latter value is an upper limit, calculated (following Zivi, 1964) for ideal annular flow. Choking may occur at considerably lower power values in case of actual annular-wavy-mist flow, but the value exceeds anyhow the homogeneous flow choking limit 170 kW.

Calculation of the vapour quality along the duct for three gravity levels (0, 1, 2-g) and three duct diameters (8.05, 16.1, 24.15 mm) at 300 K, yielded the ratio of the absolute duct lengths L_c(m) needed for full condensation under 0-g and 1-g respectively (Delil, 1992). It has been concluded that the ratio between full condensation lengths in 0-g and 1-g ranges from 1.5 for the 8.05 mm duct, via 11 for the 16.1 mm duct, up to more than 30 for the 24.15 mm duct. In other words, smaller line diameter systems are less sensitive for differences in gravity levels as compared with larger diameter systems. This is confirmed by TPX I flight data (Delil, 1995).

Since the model developed is valid for pure annular flow only, it is worthwhile to investigate the impact of other flow patterns present inside the condenser duct (mist flow at the high quality side, slug and bubbly flow at the low quality side and wavy-annular-mist in between), in other words to investigate whether the pure annular flow assumption, leads towards slightly or substantially overestimated full condensation lengths. A further complication is the lower boundary of the annular-wavy-mist flow pattern. In addition, flow pattern transitions occur at vapour quality values, which strongly depend on working fluid (temperature) and line diameter.

In summary it can be said that the information presented confirms the results of other models: When designing condensers for space applications one should carefully use and interpret data obtained from terrestrial condenser tests, even when the latter pertain to vertical down-ward flow situations (characterised by the same flow pattern). The model equations given are useful for a better understanding of the problems that can be expected: problems related to flow and heat transfer (necessary lengths of condensers for space applications). The equations and results of calculations suggest that hybrid scaling exercises, combining geometrical and fluid-to-fluid scaling, can beneficently support the design of two-phase heat transport systems for space.

With respect to the local heat transfer equation used, eq. (22), it can be remarked that it has a wrong lower limit $h \rightarrow 0$ for $(dp/dz)_t \rightarrow 0$, which disappears by incorporating conduction through the liquid layer. Preliminary calculations indicate that the incorporation of pure conduction will lead to somewhat shorter full condensation lengths, both for zero-g and for non-zero-g conditions. This implies quantitative changes only, in other words the conclusions presented above remain valid.

6. FLOW PATTERN ASPECTS

Accurate knowledge of the gravity level dependent two-phase flow regimes is crucial for modelling and designing two-phase heat transport systems for space, as flow patterns directly affect thermal hydraulic characteristics of two-phase flow and heat transfer. Therefore flow pattern (regime) maps are to be created, preferably in the non-dimensional format of figure 12.

Hamme & Best (1997) created, based on many low-gravity aircraft flight data of a R12, 10.5 mm lines experiment, three- dimensional flow pattern maps as shown in the figures 17 and 18. Figure 19 summarises their 0-g data. Figure 20 depicts data of experiments in low-g aircraft with Cyrène, an ammonia system with a 4.7 mm line diameter (Lebaigue et al., 1998). Figure 21 shows the 0-g map, derived from the TPX I VQS flight data, presented in figure 3.

The above maps partly contradict each other. A comparison between the figures suggests that the transition to annular flow occurs in these three systems more or less at the same j_v-value 0.2-0.25 m/s, but at different j_l-values. This can be caused either by the different working fluids (R12/ammonia/ammonia) or the different inner line diameter (10.5 mm/4.7 mm/4.93 mm).

It is obvious that a lot of work has to be done before such flow pattern (regime) maps will be produced and become mature, preferably in the normalised format of figure 12 or in the good alternative: the three-dimensional format j_v - j_l - g, like in the figures 17 and 18.

NOMENCLATURE

A	area	m^2
Bo	boiling number	-
Cp	specific heat at constant pressure	J/kg.K
D	diameter	m
d	diameter of curvature	m
Eu	Euler number	-
Fr	Froude number	-
g	gravitational acceleration	m/s^2
H	enthalpy	J/kg
h	heat transfer coefficient	$W/m^2.K$
h_{lv}	latent heat of vaporisation	J/kg
j	superficial velocity	m/s
k	thermal conductivity	W/m.K
L	length	m
Ma	Mach number	-
Mo	Morton number	-
$\dot{m}$	mass flow rate	kg/s
Nu	Nusselt number	-
p	pressure	Pa, N/m^2
Pr	Prandtl number	-
Q	power	W
q	heat flux	W/m^2
Re	Reynolds number	-
S	slip factor	-
T	temperature	K, $^\circ$C
t	time	s
v	velocity	m/s
We	Weber number	-
X	vapour quality	-
z	axial or vertical co-ordinate	m
α	vapour fraction (volumetric)	-
β	constant in eq. (13)	-
δ	surface roughness	m
Δ	difference, drop	-
μ	viscosity	Ns/m^2
σ	surface tension	N/m
π	dimensionless number	-
ρ	density	kg/m^3
ν	angle (with respect to gravity)	rad

Subscripts

a	acceleration	p	pore/prototype
c	condenser	s	entropy
f	friction	t	total
g	gravitation	tp	two-phase
l, ℓ	liquid	v	vapour
m	momentum, model	w	water
o	reference condition		

REFERENCES

1. Amadieu, M. et al., 1997, Development of a Deployable Radiator using a LHP as Heat Transfer Element, ESA SP400, *6th European Symp. on Space Environmental Control Systems*, Noordwijk, Netherlands, 283-288.

2. Antoniuk, D. & Nienberg, J., 1998, Analysis of Salient Events in the Two-Phase Thermal Control Flight Experiment, SAE 981817, *28th Int. Conf. on Environmental Systems*, Danvers, USA.
3. Bienert, W. & Wolf, D., 1995, Temperature Control with Loop Heat Pipes: Analytical Model and Test Results, *9th Int. Heat Pipe Conf.* Albuquerque, USA, 981-988.
4. Bienert, W. & Baker, C. & Ducao, A., 1998, Loop Heat Pipe Flight Experiment, SAE 981580, *28th Int. Conf. on Environmental Systems*, Danvers, USA.
5. Butler, D. et al., J., 1995, Flight Testing of the Capillary Pumped Loop Flight Experiments, SAE 951566, *25th Int. Conf. on Environmental Systems*, San Diego, USA.
6. Chen, I. et al., 1991, Measurements and Correlation of Two-Phase Pressure Drop under Microgravity Conditions, *J. of Thermophysics*, 5, 514-523.
7. Cullimore, B., 1993, Capillary Pumped Loop Application Guide, SAE 932156, *23rd Int. Conf. on Environmental Systems*, Colorado Springs, USA.
8. Cullimore, B. & Nikitkin, M., 1997, CPL and LHP Technologies: What are the differences, What are the similarities?, SAE 981587, *28th Int. Conf. on Environmental Systems*, Danvers, USA.
9. Dam, A.A. ten & Berg, J.I. van den, 1992, Numerical simulation of a condenser in two-phase heat transport systems, a feasibility study, NLR TP 92081.
10. Da Riva, I. & Sanz. A., 1991, Condensation in Ducts, *Microgravity Science and Technology*, 4 , 179-187.
11. Delil, A.A.M., 1987, Moveable Thermal Joints for Deployable or Steerable Spacecraft Radiator Systems, NLR MP 87016, SAE 871460, *17th Intersoc. Conf. on Environmental Systems*, Seattle, USA.
12. Delil, A.A.M., 1988, A Sensor for High-Quality Two-Phase Flow, NLR MP 88025, *16th Int. symposium on Space Technology and Science*, Sapporo, Japan, 957-966.
13. Delil, A.A.M., 1991, Thermal gravitational modelling and scaling of two-phase heat transport systems: Similarity considerations and useful equations, predictions versus experimental results, NLR TP 91477, ESA SP-353, *Europ. Symp. Fluids in Space*, Ajaccio, France, 579-599.
14. Delil, A.A.M., 1992, Gravity dependence of pressure drop and heat transfer in straight two-phase heat transport system condenser ducts, NLR TP 92167, SAE 921168, *22nd Int. Conf. on Environmental Systems*, Seattle, USA.
15. Delil, A.A.M. et al., 1995, TPX for In-Orbit Demonstration of Two-Phase Heat Transport Technology - Evaluation of Flight & Postflight Experiment Results, NLR TP 95192, SAE 95150, *25th Int. Conf. on Environmental Systems*, San Diego, USA.
16. Delil, A.A.M. & Dubois, M. & Supper, W., 1997, The European Two-Phase Experiments TPX I & TPX II, NLR TP 97502, *10th Int. Heat Pipe Conf.*, Stuttgart, Germany.
17. Delil, A.A.M. et al., Sensors and Components for Aerospace Thermal Control, Life Science and Propellant Systems, NLR TP 97504, *AIP387 Conf. on Applications of Thermophysics in Microgravity, Space Technology & Applications Int. Forum*, Albuquerque, USA.
18. Delil, A.A.M., 1998, Two-Phase Heat Transport Systems for Space: Thermal Gravitational Modelling & Scaling, Similarity Considerations, Equations, Predictions, Experimental Data and Flow Pattern Mapping, NLR TP 98268, SAE 981692, *28th Int. Conf. on Environmental Systems*, Danvers, USA.
19. Dunbar, N. & Siepmann, R. & Supper, W., 1990, European Two-Phase Heat Transport Technology Test Bed Results, SAE 901271, *20th Int. Conf. on Environmental Systems*, Williamsburg, USA.
20. Dunbar, N., 1996, ATLID Laser Head Thermal Control Design and Development of a Two-Phase Heat Transport System for Practical Application, SAE 961561, *26th Int. Conf. Environmental Systems*, Monterey, USA.
21. Geraets, J.J.M., 1986, Centrifugal scaling of iso-thermal gas-liquid flow in horizontal tubes, Techn. Univ. Delft.
22. Hagood, R., 1998, CCPL Flight Experiment: Concepts through Integration, SAE 981694, 28th Int. Conf. on Environmental Systems, Danvers, USA.
23. Hamme, T.A. & Best, F.R., 1997, Gravity Dependent Flow Regime Mapping, *AIP 387, Space Technology & Applications Int. Forum*, Albuquerque, USA, 635-640.
24. Kim, J.H., et al., 1997, The Capillary Pumped Loop III Flight Demonstration, Description, and Status, *AIP 387, Space Technology & Applications Int. Forum*, Albuquerque, USA, 623-628.
25. Ku, J. & Ottenstein, L. & Butler, D., 1996, Performance of CAPL 2 Flight Experiment, SAE 961431, *26th Int. Conf. Environmental Systems*, Monterey, USA.
26. Ku, J. & Yun, S, 1998, Design and Test Results of CAPL-3 Engineering Test Bed and Ground Test of CAPL-3 Flight Experiment, *28th Int. Conf. on Environmental Systems*, Danvers, USA.
27. Maidanik, Y. & Solodovnik, N. & Fershtater, Y., 1995, Investigation of Dynamic and Stationary Characteristics of Loop Heat Pipe, *9th Int. Heat Pipe Conf.*, Albuquerque, USA, 1002-1006.
28. Maidanik, Y. & Fershtater, Y. & Goncharov, K., 1991, Capillary Pump Loop for Systems of Thermal Regulation of Spacecraft, ESA SP 324, *4th European Symp. on Space Environmental Control Systems*, Florence, Italy, 87-92. 29. Miller-Hurlbert, K., 1997, The Two-Phase Extended Evaluation in Microgravity (TEEM) Flight Experiment: Description and Overview, *AIP. 387, Space Technology & Applications Int. Forum*, Albuquerque, USA, 547-554.
30. Orlov, A.A., et al., 1997, The Loop Heat Pipe Experiment Onboard the Granat Spacecraft. *6th European Symp. on Space Environmental Control Systems*, Noordwijk, Netherlands, 341-353.
31. Oshinowo, T. & Charles, M.E., 1974, Vertical Two-Phase Flow, Flow Pattern Correlations, *Can. J. Chem. Engng.*, 52, 25-35.
32. Ottenstein, L. & Nienberg, J., 1998, Flight Testing of Two-Phase Flow Flight Experiment, SAE 981816, *28th Int. Conf. on Environmental Systems*, Danvers, USA.
33. Soliman, M. & Schuster, J.R. & Berenson, P.J., 1968, A General Heat Transfer Correlation for Annular Flow Condensation,. *ASME C, J. Heat transfer*, 90, 267-276.
34. Stenger, F.J., 1966, Experimental study of water-filled capillary pumped heat transfer loops, NASA X-1310.
35. Zivi, S.M., 1964, Estimation of Steady-State Void Fraction by Means of the Principle of Minimum Entropy Production, *ASME C, J. Heat Transfer*, 86, 247-252.

Table 1 Relevance of π-numbers for thermal Gravitational scaling of two-phase loops	Liquid Parts		Evaporators Swirl & Capillary	Non-liquid Lines Vapour/2-Phase	Condensers
	Adiabatic	Heating/Cooling			
π_1 = D/L = geometry	•	•	•	•	•
$\pi_2 = Re_l = (\rho vD/\mu)_l$ = inertia/viscous	•	•	•	•	•
$\pi_3 = Fr_l = (v^2/gD)_l$ = inertia/gravity	•	•	•	/•	•
$\pi_4 = Eu_l = (\Delta p/\rho v^2)_l$ = pressure head/inertia	•	•	•	•	•
π_5 = cos ν = orientation with respect to g	•	•	•	/•	•
π_6 = S = slipfactor = v_v/v_l			•	•	•
π_7 = density ratio = ρ_v/ρ_l			•	•	•
π_8 = viscosity ratio = μ_v/μ_l			•	•	•
$\pi_9 = We_l = (\rho v^2 D/\sigma)_l$ = inertia/surface tension			•	/•	•
$\pi_{10} = Pr_l = (\mu Cp/k)_l$		•	•		•
$\pi_{11} = Nu_l = (hD/k)_l$ = convective/conductive		•	•		•
$\pi_{12} = k_v/k_l$ = thermal conductivity ratio			•		•
$\pi_{13} = Cp_v/Cp_l$ = specific heat ratio			•		•
$\pi_{14} = \Delta H/h_{lv}$ = enthalpy number = X = quality		•	•	•	•
$\pi_{15} = Mo_l = (\rho_l \sigma^3/\mu_l^4\, g)$ = capillarity/buoyancy			•	/•	•
$\pi_{16} = Ma = v/(\partial p/\partial \rho)^{1/2}{}_s$			•	•	•
$\pi_{17} = (h/k_l)(\mu_l^2 g)^{1/3}$			•		•
$\pi_{18} = L^3 \rho_l^2\, g\, h_{lv}/k_l \mu_l (T-T_o)$			•		•

CL Capillary Link CLH CL Header Q_{COND} Condenser Imbalancing Power

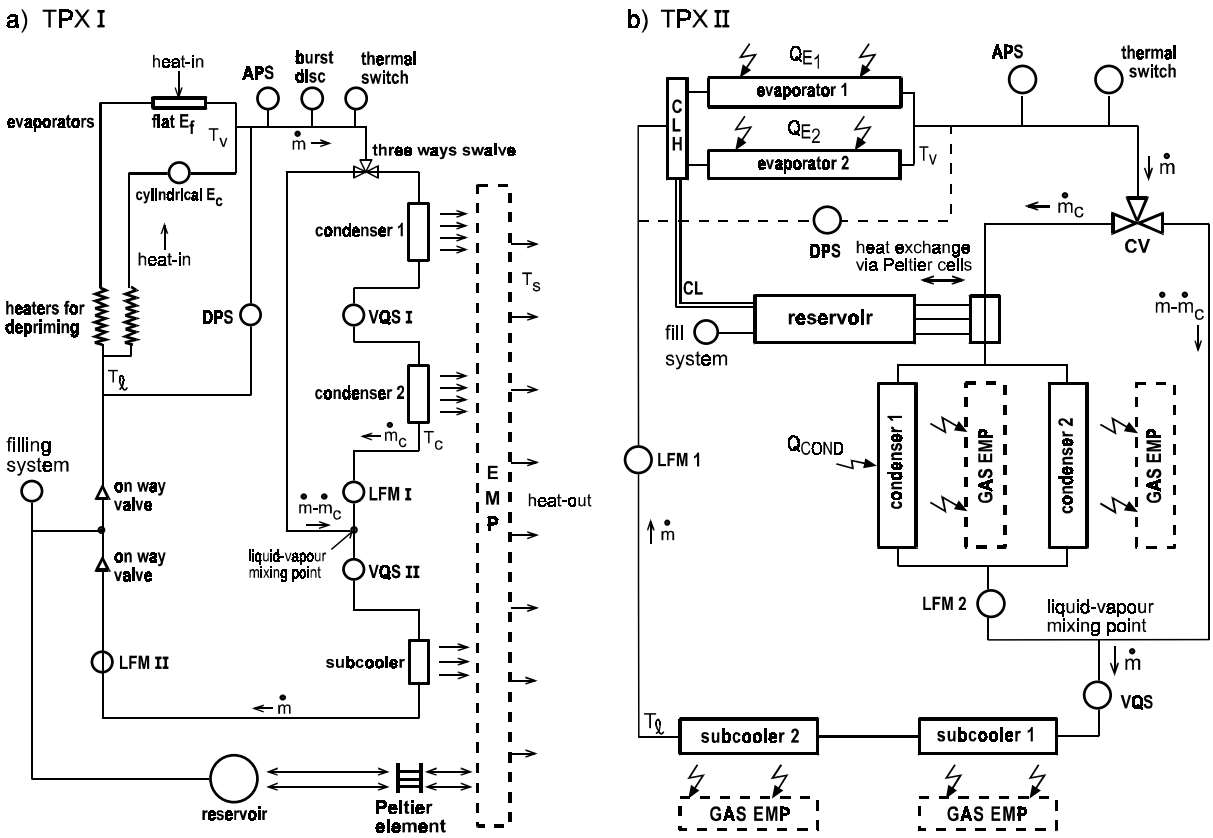

Fig. 1 Schematics of TPX I and TPX II

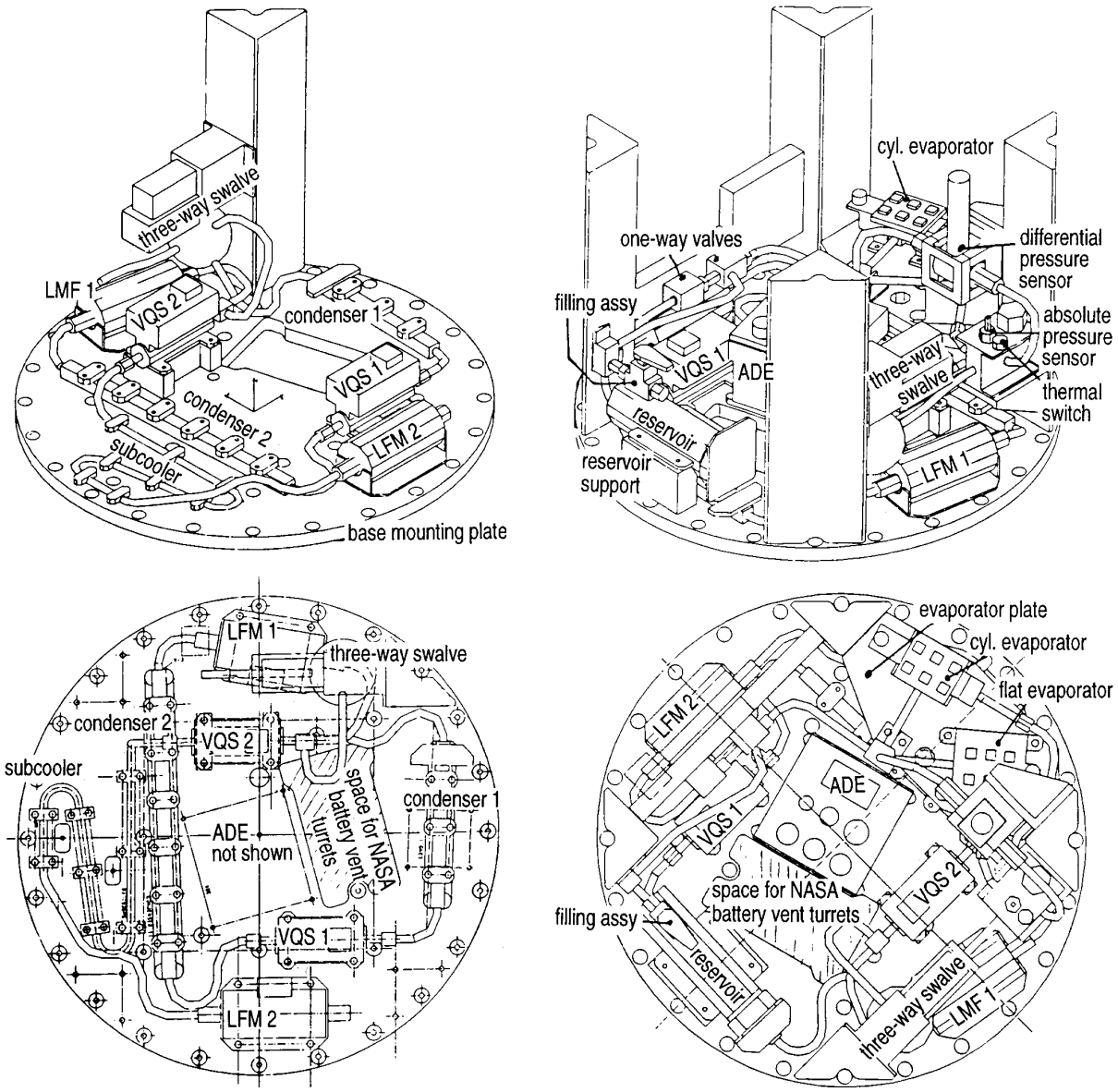

Fig. 2 TPX I Lay out

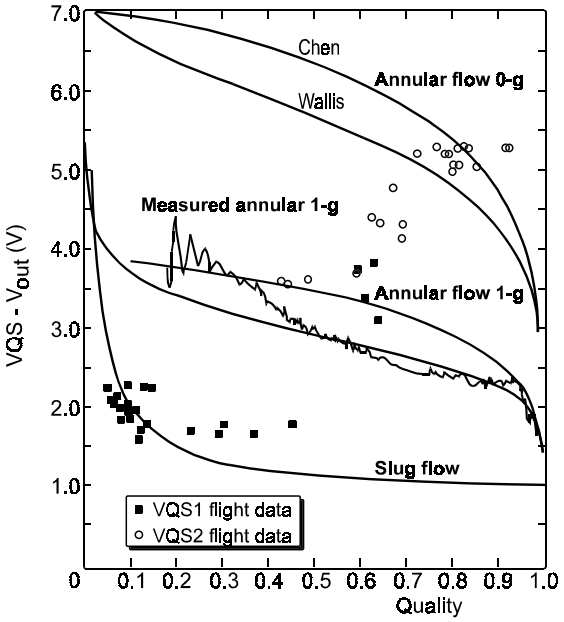

Fig. 3 VQS Theoretical Responses and Test Data

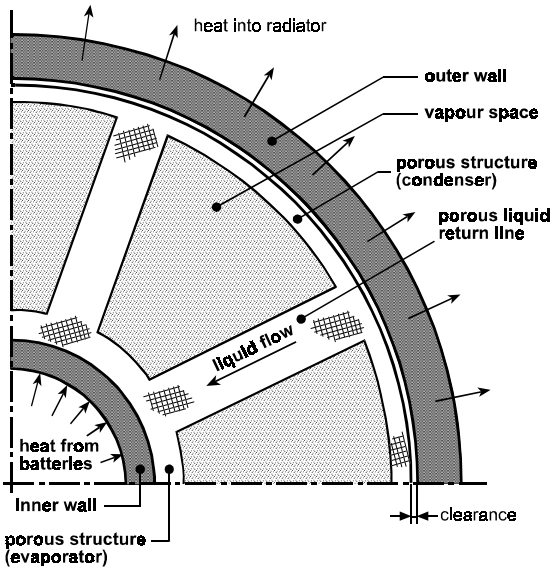

Fig. 5 Cross-section of a Radial Heat Pipe Joint

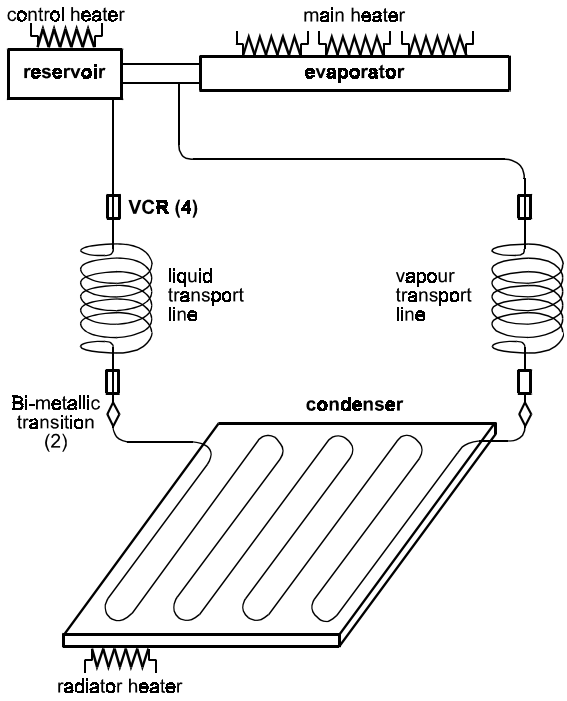

Fig. 4 Loop Heat Pipe Schematic

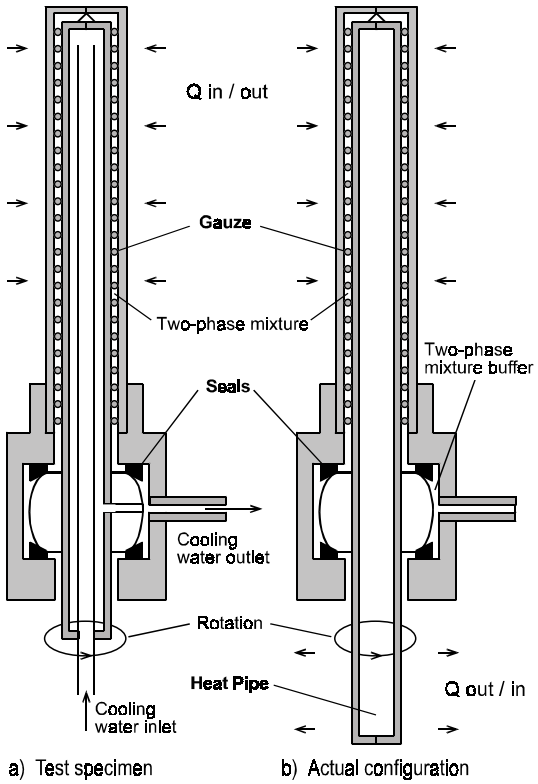

Fig. 6 Rotatable Radial Heat Pipe Joint

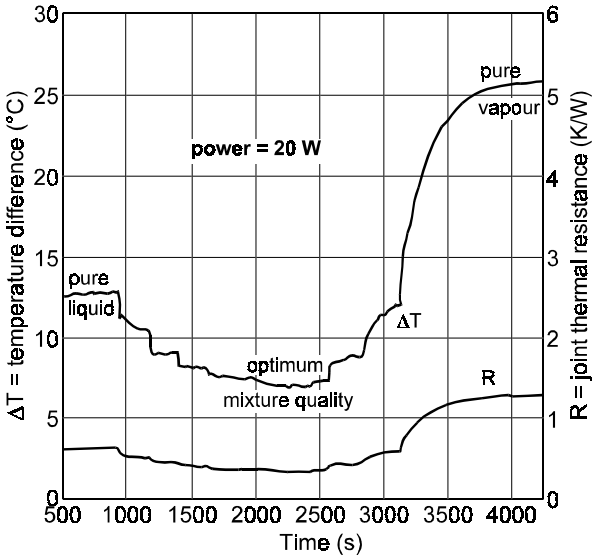

Fig. 7 Determination of Optimum Filling

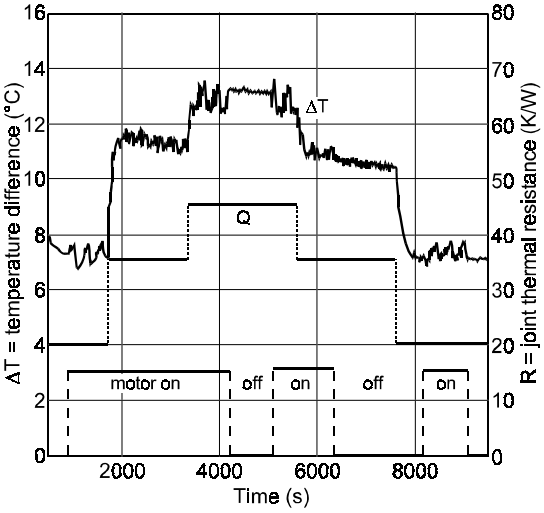

Fig. 8 Power Dependence of Joint Resistance (non-rotating and rotating at 17.5 rpm)

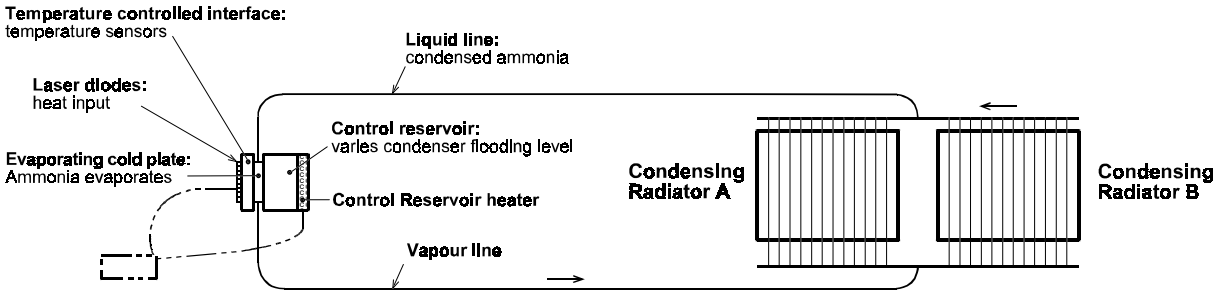

Fig. 9 ATLID Laser Head Thermal Control Schematic

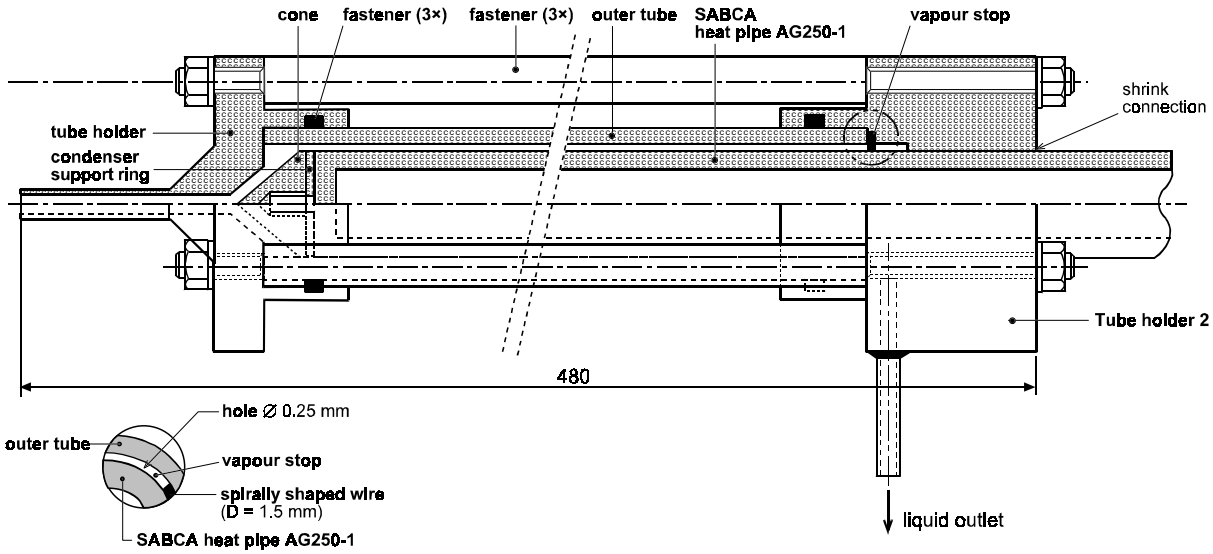

Fig. 10 High Efficiency Low Pressure Drop Condenser

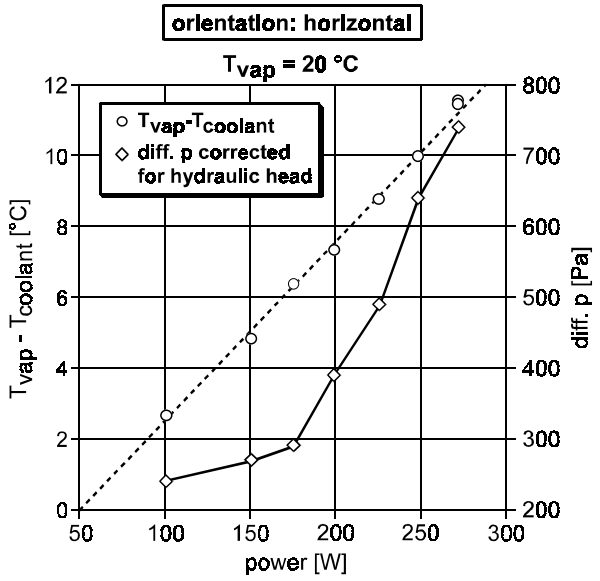

Fig. 11 Temperature and Pressure Drops as a Function of Power

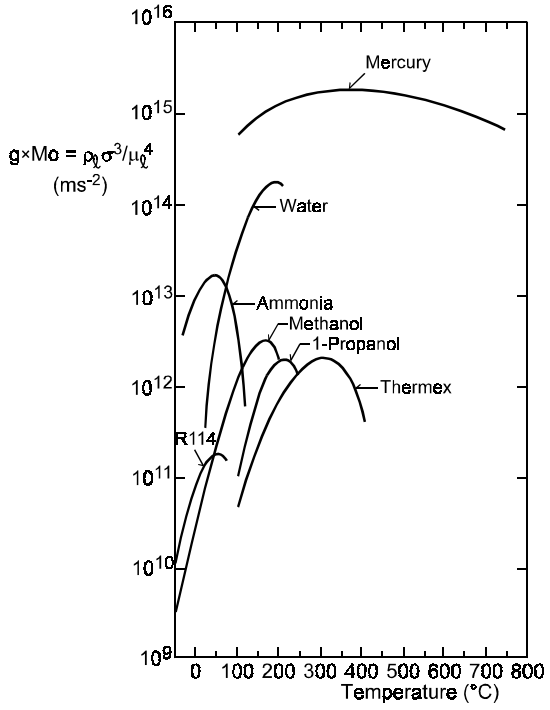

Fig. 13 The Grouping $\rho_\ell \sigma^3/\mu_\ell^4$ for Various Fluids, as a Function of the Temperature

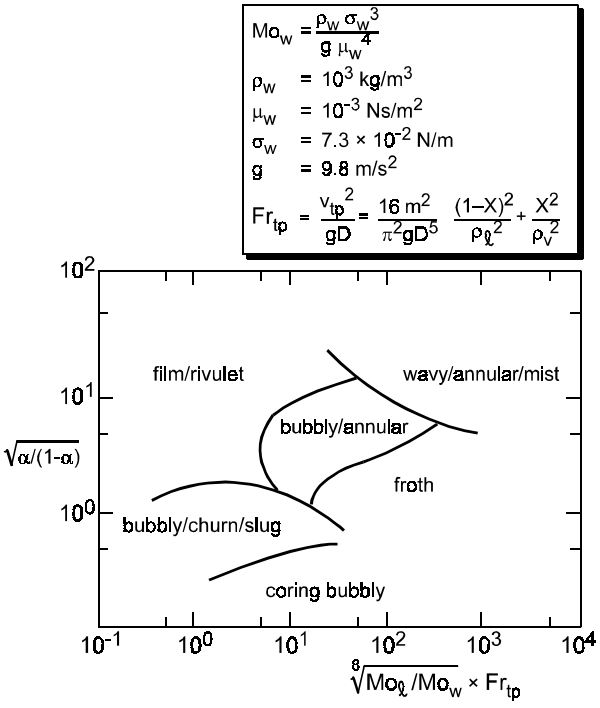

Fig. 12 Flow Pattern Map for Vertical Downward Flow

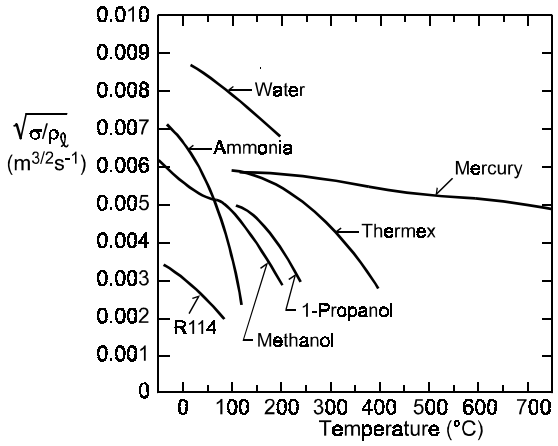

Fig. 14 $\sqrt{\sigma/\rho_\ell}$ versus Temperature for Various Fluids

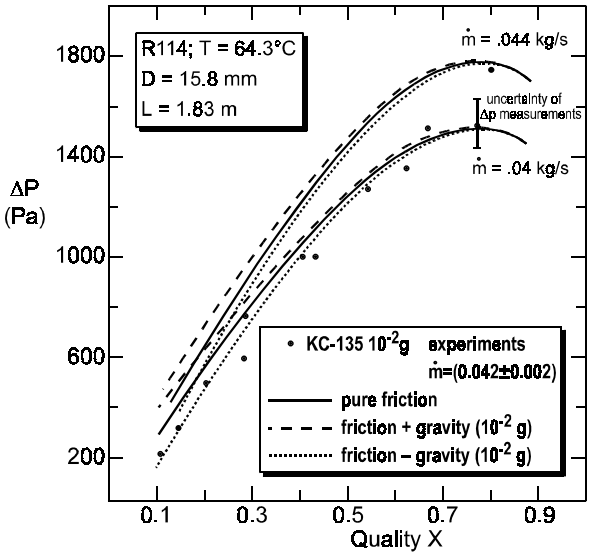

Fig. 15 Comparison of Measured and Predicted Adiabatic Pressure Drops for a R114 Duct

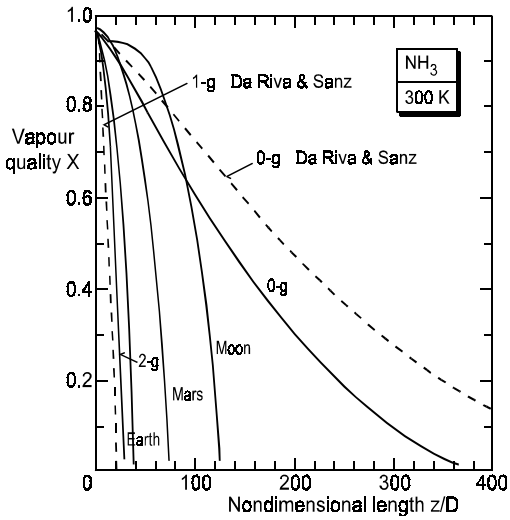

Fig. 16 Vapour Quality along the 16.1 mm Duct for Ammonia at 300 K (1000 W, ΔT = 10 K), for All Gravity Levels

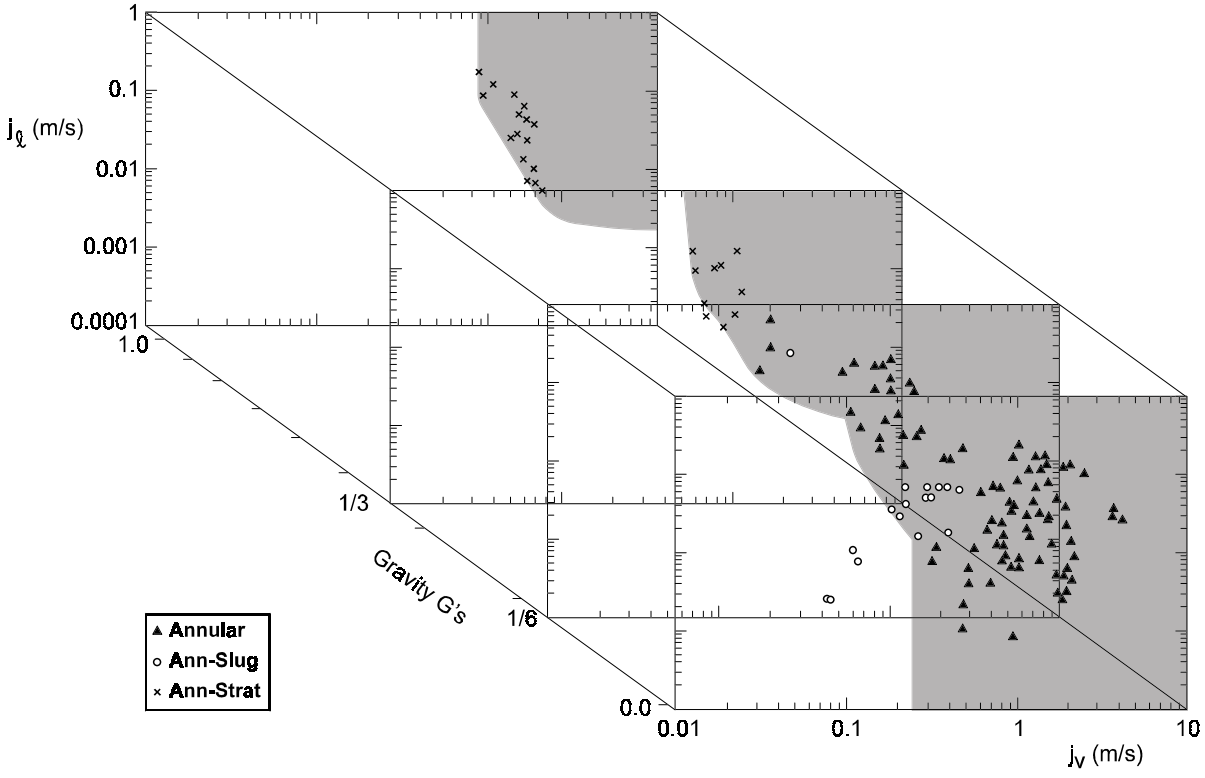

Fig. 17 3-D Flow Regime as a Function of Gravity Dependent Annular Flow Map

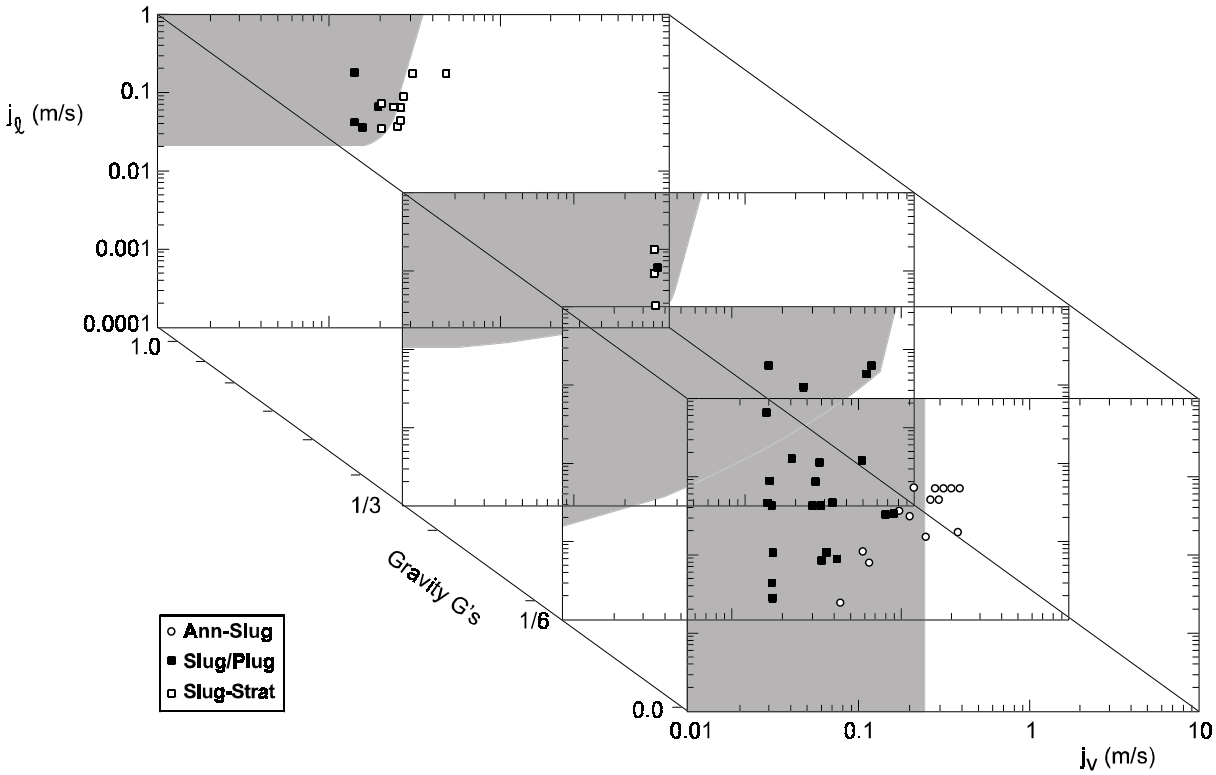

Fig. 18 3-D Flow Regime as a Function of Gravity Dependent Slug/Plug Flow Map

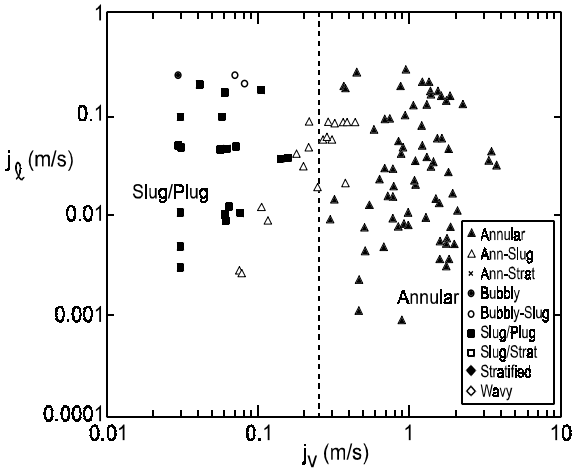

Fig. 19 Flow Regime Map in Microgravity (~0 G)

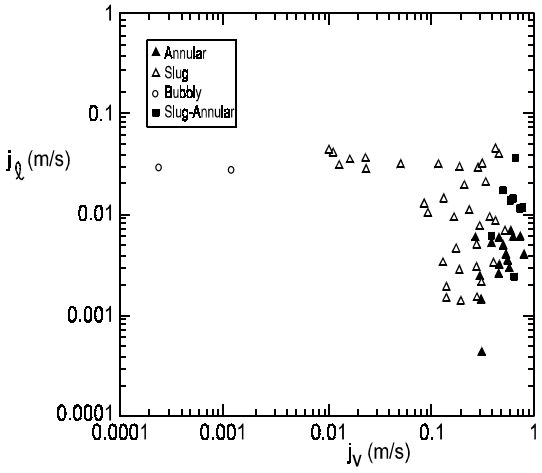

Fig. 20 Cyrène Flow Pattern Map

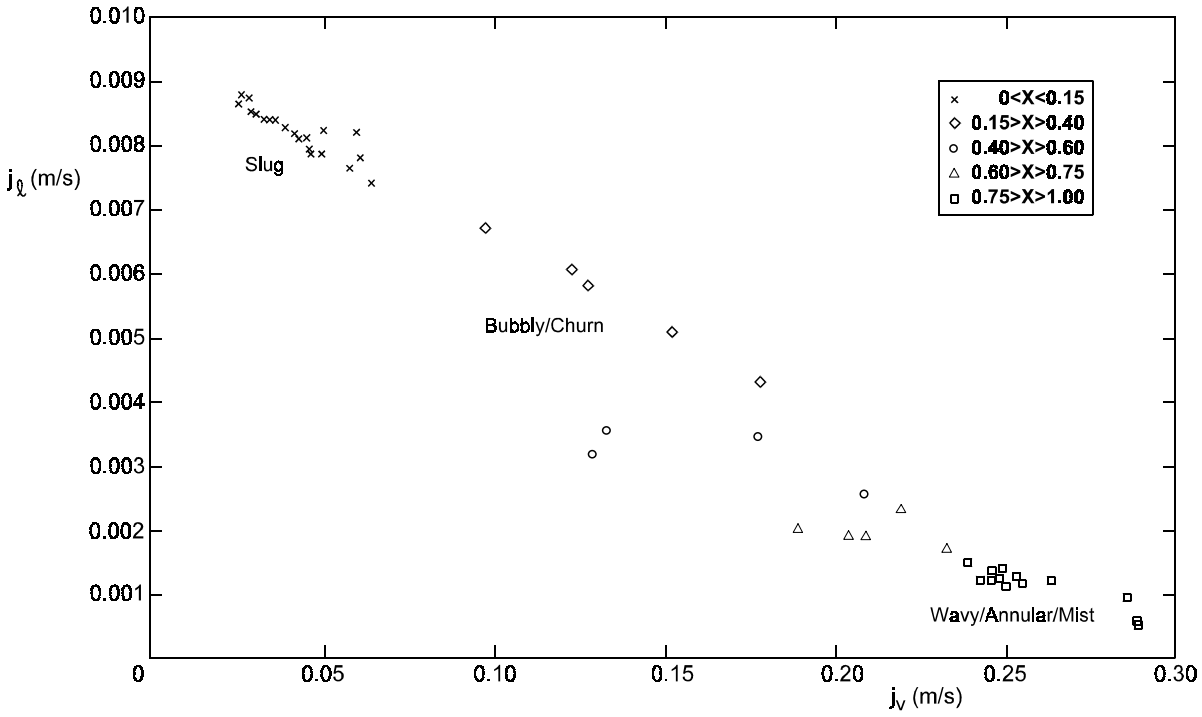

Fig. 21 Flow Patterns Derived from TPX I VQS Flight Data